Tectonics

RESEARCH ARTICLE
10.1029/2018TC005192

Key Points:
- Early-Middle Jurassic extensional tectonics in the Arabian margin is described
- Syn-sedimentary faults occur in the Arabian domain and in the Radiolarite Basin
- Tectonically driven drowning of the Triassic to Early Jurassic carbonate platform

Correspondence to:
S. Tavani,
stefano.tavani@unina.it

Citation:
Tavani, S., Parente, M., Vitale, S., Iannace, A., Corradetti, A., Bottini, C., et al. (2018). Early Jurassic rifting of the Arabian passive continental margin of the Neo-Tethys. Field evidence from the Lurestan region of the Zagros fold-and-thrust belt, Iran. *Tectonics*, *37*, 2586–2607. https://doi.org/10.1029/2018TC005192

Received 20 JUN 2018
Accepted 17 JUL 2018
Accepted article online 30 JUL 2018
Published online 13 AUG 2018

Early Jurassic Rifting of the Arabian Passive Continental Margin of the Neo-Tethys. Field Evidence From the Lurestan Region of the Zagros Fold-and-Thrust Belt, Iran

Stefano Tavani[1], Mariano Parente[1], Stefano Vitale[1], Alessandro Iannace[1], Amerigo Corradetti[1], Cinzia Bottini[2], Davoud Morsalnejad[3], and Stefano Mazzoli[1]

[1]DiSTAR, Università degli Studi di Napoli Federico II, Naples, Italy, [2]Dipartimento di Scienze della Terra, Università degli Studi di Milano, Milan, Italy, [3]N.I.O.C, Tehran, Iran

Abstract The Arabian passive margin formed at the southern margin of the Neo-Tethys ocean during the breakup of Pangea. In the Lurestan region of the Zagros mountain belt, the deformed Arabian continental paleo-margin can be reconstructed as originally consisting of distinct crustal domains, including a proximal sector and a distal continental ribbon, separated by a deep-water trough, known as the Radiolarite Basin. Such an architecture was shaped by the continental rifting process, thus reflecting timing and style of continent separation, which is generally assumed to have occurred during the Permo-Triassic interval. This study reports evidence of syn-sedimentary extensional faults, unconformities, and facies changes in the Mesozoic stratigraphic succession of the Lurestan region, which point to a major Jurassic extensional pulse. In detail, extension reached its climax at the end of the Early Jurassic, when tectonically driven drowning of the long-lived Triassic to Early Jurassic carbonate platform led to the transition from shallow- to deep-water environments in large areas of the inner margin, coevally with the development of the Radiolarite Basin. Our findings suggest a two-step continental rifting in this area, with the first Permo-Triassic phase predating an Early Jurassic one.

1. Introduction

The Zagros mountain belt formed as part of the Alpine-Himalayan orogenic system (Figure 1a) as consequence of the closure of the Neo-Tethys Ocean and of the following continental collision between the Arabian and Eurasian plates (e.g., Agard et al., 2005, 2011; Alavi, 1991, 1994; Berberian, 1995; Berberian & King, 1981; Braud, 1987; Dercourt et al., 1986; Frizon de Lamotte et al., 2011; McQuarrie & van Hinsbergen, 2013; Molinaro et al., 2005; Ricou et al., 1977; Stampfli & Borel, 2002; Stöcklin, 1968). The tectonic architecture of the Zagros belt is strongly controlled by different kinds of sedimentary and structural inheritances, including (i) lateral facies changes, producing important lateral variations of the mechanical properties of the multilayer, and (ii) faults previously formed within the Arabian plate, spanning in age from the Precambrian to the Mesozoic (e.g., Alavi, 1994, 2004; Bahroudi & Koyi, 2003; Berberian, 1995; Hessami et al., 2001; Jackson, 1980; Mouthereau et al., 2012; Sherkati & Letouzey, 2004; Sherkati et al., 2005; Stöcklin, 1968; Talbot & Alavi, 1996; Tavakoli-Shirazi et al., 2013). Preexisting structures include those developed during the rifting stage, which eventually led to the opening of the Neo-Tethys Ocean. In fact, the major terrains currently forming the collisional system coincide with the major lithospheric domains inherited from the Neo-Tethyan rifting event (e.g., Ghasemi & Talbot, 2006; Robertson, 2007; Saccani et al., 2013; Vergés et al., 2011). In detail, the Zagros orogeny deformed the Arabian margin, which was the southern passive margin of the southern branch of the Neo-Tethys (Berberian & King, 1981; Blanc et al., 2003; Mouthereau et al., 2012; Sepehr & Cosgrove, 2004; Vergés et al., 2011; Wrobel-Daveau et al., 2010). The Zagros belt is bounded to the NE by the Main Recent Fault and the Main Zagros Thrust (Figure 1a), interpreted by most authors as the Neo-Tethys suture zone (e.g., Ghasemi & Talbot, 2006). The Kermanshah, Neyriz, and Nain-Baft ophiolitic complexes (e.g., Moghadam & Stern, 2011, 2015) are exposed along this suture, with the Sanandaj-Sirjan sector to the NE of this domain being considered as the northern continental margin of the southern branch of the Neo-Tethys (Figure 1b; e.g., Blanc et al., 2003; Ghasemi & Talbot, 2006; Robertson, 2007; Saccani et al., 2013; M. A. Ziegler, 2001). Alternatively,

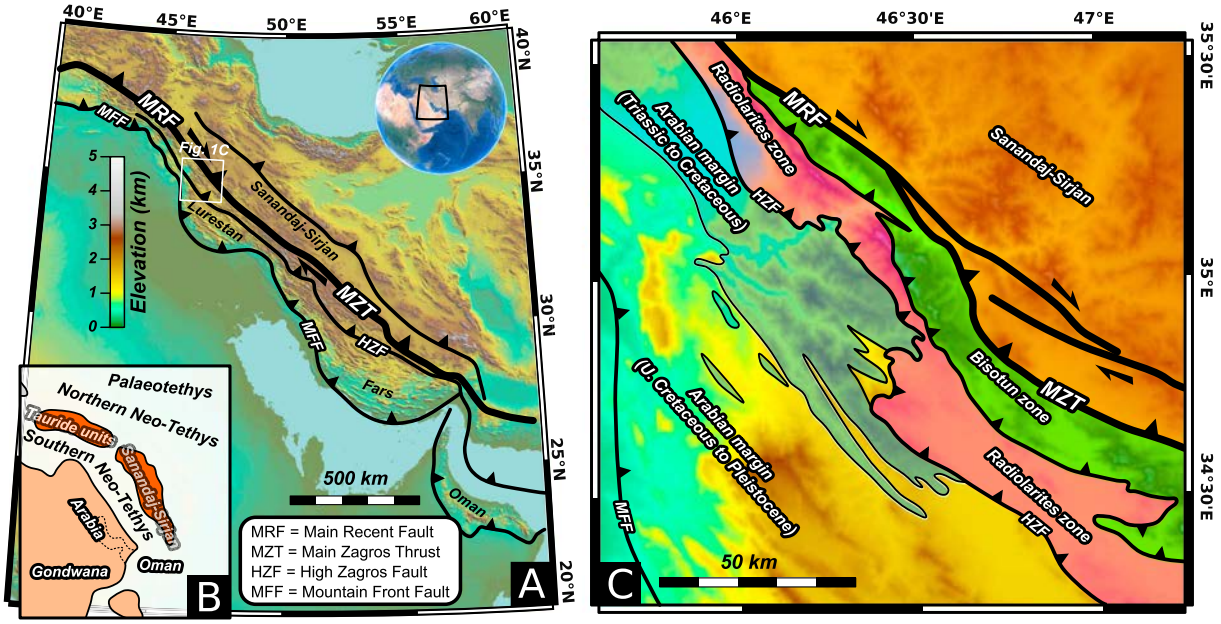

Figure 1. The Zagros Belt in the Lurestan area. (a) Structural scheme of the Zagros Mts., with (b) paleogeographic reconstruction at Jurassic time (modified from Saccani et al., 2013). (c) Simplified scheme of the NW portion of the Lurestan area (after Sadeghi & Yassaghi, 2016).

Alavi (1994) suggested an Arabian affinity for the Sanandaj-Sirjan Domain, with a complex reimbrication history of the ophiolitic complexes presently interposed between the Zagros and the Sanandaj-Sirjan Domain. Not only the location of the suture is uncertain but also timing, duration, and evolution of the rifting events that led to the development of the above mentioned southern branch of the Neo-Tethys have not been fully clarified too. A Permian to Early Triassic age is commonly inferred for the onset of rifting based on (i) differences in the Permo-Triassic stratigraphic succession of the various crustal blocks (e.g., Alavi, 1980; Berberian & King, 1981; Ghasemi & Talbot, 2006), (ii) occurrence of a regionally relevant unconformity (e.g., James & Wynd, 1965; Koop & Stoneley, 1982; Szabo & Kheradpir, 1978), (iii) age of the volcanic activity (e.g., Ghasemi & Talbot, 2006), and (iv) paleomagnetic data from the different crustal blocks of the area (e.g., Muttoni et al., 2009). However, a clear breakup unconformity is lacking in the Arabian Margin, whose tectono-stratigraphic architecture does not completely fit the classic syn-rift-breakup-postrift sequence (e.g., Franke, 2013). The onset of deep-water sedimentation in the radiolarite-dominated basins flanking to the NE the passive margin started during the late Early Jurassic (Kermanshah Radiolarite basin, Gharib & De Wever, 2010; Pichakun basins, Robin et al., 2010), thus being significantly delayed with respect to the inferred age of the breakup. Jurassic and Cretaceous pulses of extensional activity, which were able to produce even mantle exhumation, are also documented within the Arabian margin (e.g., Wrobel-Daveau et al., 2010). This is not in line with a simple postrift thermal subsidence of the margin. The occurrence of ophiolitic complexes exposed along the suture does not permit to solve the issue of continental breakup. In fact, such complexes are for the vast majority Cretaceous in age and have mostly formed in suprasubduction, intraoceanic island arc settings, with very rare Late Triassic ages documented (e.g., Moghadam & Stern, 2015; Robertson, 2007). In addition, and with very few exceptions (Jahani et al., 2009; Sepehr & Cosgrove, 2004), no evidence of Permo-Triassic syn-sedimentary faults occurs in the stratigraphic record of the Zagros, making it difficult to clearly define the duration of the continental rifting stage.

The Lurestan Province in Iran is one of the few places of the Zagros mountain belt where Triassic and Jurassic rocks are largely exposed. They belong to various nappes and thrust sheets made at the expenses of different domains of the Arabian passive margin (Figure 1c). The aim of this work is to shed light on the extensional deformation recorded in the Arabian passive margin by reporting on major facies and thickness changes, syn-sedimentary faults, and angular unconformities of the Triassic-Jurassic succession of the area. These features provide strong geological evidence for an Early Jurassic rifting phase and new constraints to refine geodynamic models for the breakup of Pangea in the Zagros area.

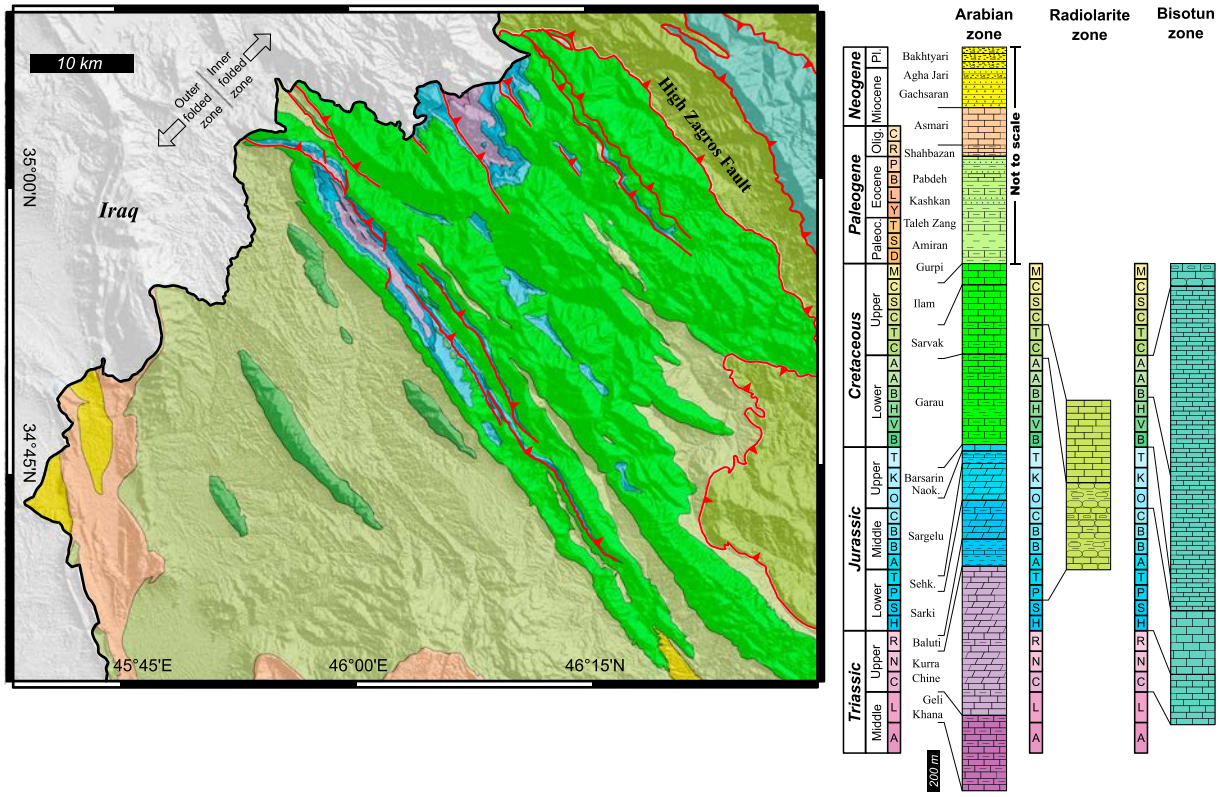

Figure 2. Geological map of the NW portion of the Lurestan area, showing the stratigraphic successions of the three distinct Mesozoic domains of the study area. The stratigraphic columns for the Radiolarite and Bisotun domains are simplified after Wrobel-Daveau et al. (2010), Gharib and De Wever (2010), Abdi et al. (2014), and Sadeghi and Yassaghi (2016).

2. Geological Setting

The study area is located along the NW portion of the Lurestan orogenic arc, which is a major salient of the Late Cretaceous to Cenozoic, mainly NW-SE striking Zagros mountain belt (Figure 1a; Alavi, 1991, 2007; Koshnaw et al., 2017; Lacombe et al., 2011; Mouthereau et al., 2012; Vergés et al., 2011). This arc is located between the Kirkuk and Dezful embayments to the NW and SE, respectively, and is bounded to the NE by the previously mentioned Main Recent Fault and Main Zagros Fault (Figure 1a). These two lithospheric faults separate terrains of the former Arabian margin to the SW from those of the Sanandaj-Sirjan block to the NE. Folds and thrusts of the Lurestan region are generally NW-SE striking and SW-verging, turning to NNW-SSE and E-W striking at the northwestern and southeastern boundary of the Lurestan arc, respectively (e.g., Casini et al., 2017; Tavani et al., 2018). Two main tectonic contacts (nappe boundaries) occur in the northern portion of the study area (Sadeghi & Yassaghi, 2016; Figure 1c), the southwestern one being known as the High Zagros Fault. These major boundaries define three tectonic zones: (i) Arabian, (ii) Radiolarite, and (iii) Bisotun, corresponding to three different Mesozoic domains (e.g., Barrier & Vrielynck, 2008; Braud, 1987; Ricou et al., 1977; Vergés et al., 2011). The Arabian zone complex forms the structurally lowermost tectonic unit, and it is made of rocks of the inner portion of the Arabian passive margin. Tectonically on top of this, the Radiolarite nappe consists of Mesozoic sediments originally deposited within the Kermanshah Radiolarite Basin (Kazmin et al., 1986; Navabpour et al., 2011; Wrobel-Daveau et al., 2010). These deep-water sediments were deposited on thinned continental crust of the Arabian margin and, partly, on top of exhumed subcontinental mantle (Wrobel-Daveau et al., 2010). To the NE, the Radiolarite nappe is overthrust by the Mesozoic carbonates of the Bisotun unit, which during the Mesozoic was flanking to the NE the Radiolarite Basin (Braud, 1987; Ricou et al., 1977), thus forming a distal continental ribbon interposed between the Neo-Tethys ocean and the Kermanshah Radiolarite Basin (Figures 1c and 2).

Figure 3. Triassic units. Panoramic view of NE-dipping strata of the Geli Khana and Kurra Chine Fms. (inset shows the location of the exposure).

2.1. The Arabian Complex

The Arabian complex includes a folded, thick sedimentary pile, and it is further divided into two areas, that is, the inner- and outer-folded belt zones (Figures 1c and 2). These represent remnants of the proximal and distal zones of the former Arabian passive margin, respectively (Vergés et al., 2011). The outer-folded belt exposes mostly Upper Cretaceous to Cenozoic rocks, whereas in the northeastern inner-folded belt, Triassic to Cretaceous rocks are widespread. Both areas are characterized by NW-SE striking folds, showing wavelengths ranging from 2 to 10 km (Casciello et al., 2009; Saura et al., 2011; Vergés et al., 2011). The Mesozoic stratigraphic successions of the two zones are similar, with the remarkable exception of the Lower Cretaceous portion (Garau Fm.). The thickness of this part of the Mesozoic multilayer is about 200–300 m in the inner part of the margin (outer-folded belt) and increases to the NE (Sadeghi & Yassaghi, 2016) where, according to our field observations, it exceeds 1 km. Such thickness variation of the Lower Cretaceous Garau Fm. is coherent with regional data reported by Bordenave and Hegre (2010), who estimated a minimum and maximum thickness for this formation of 350 and 700 m, respectively. With few exceptions, Cenozoic sedimentary rocks do not occur in the inner-folded belt, which is uplifted with respect to the southern one by at least 2 km (Figures 1c and 2).

The stratigraphy of the Triassic-Jurassic rocks of the Arabian Margin of NW Lurestan, which is schematically illustrated in Figure 2, is mainly based on formations that have their type sections in the Iraqi portion of the Zagros belt and have been formally described in the Stratigraphic Lexicon of Iraq (van Bellen et al., 1959). Further information is given in James and Wynd (1965). The oldest exposed rocks, which crop out only in the northern portion of the area, belong to the Anisian-Ladinian Geli Khana Fm., consisting of 450-m-thick thin-bedded shallow-water limestones, calcareous shales, and dolostones (Figures 2 and 3). It is overlain by the Carnian-Norian shallow-water Kurra Chine Fm., which is about 700 m thick (Figures 2 and 3) and consists of thick-bedded dolostones and limestones, with intervals made of thin-bedded marls, argillaceous limestones, and dolostones. The overlying Baluti Shale Fm., of Upper Triassic age (Norian-Rhaetian?), consists of dark gray to black shales, with tens of centimeters-thick intercalations of dolomitic limestones, deposited in continental to coastal marine conditions. Its thickness is roughly 100 m (Figures 2 and 4). The overlying Upper Triassic-Lower Jurassic (upper Norian?-Rhaetian to Pliensbachian) Sarki Fm. and Sehkaniyan Fm., of Lower Jurassic age (upper Pliensbachian-Toarcian), consist mostly of shallow-water dolostones, having a thickness of nearly 200 and 100 m, respectively (Figure 4). The lithostratigraphic package including Baluti Shales, Sarki, and Sehkaniyan Fms. displays gradual thickness variations across the area, as seen in the examples of Figure 4, where the thickness computed by means of 3-D layers reconstruction (e.g., Snidero et al., 2011) is shown. The cumulative thickness of the package ranges from 350 to almost 550 m, and most of the variation is attributable to thickness variations occurring in the Sehkaniyan and Baluti Shales Fms. The Sehkaniyan Fm. is overlain by the Lower to Middle Jurassic (Toarcian?-Callovian) Sargelu Fm. (Figures 2 and 4a), consisting of shales, marls, and marly limestones of outer ramp to basin facies. The deposition of the

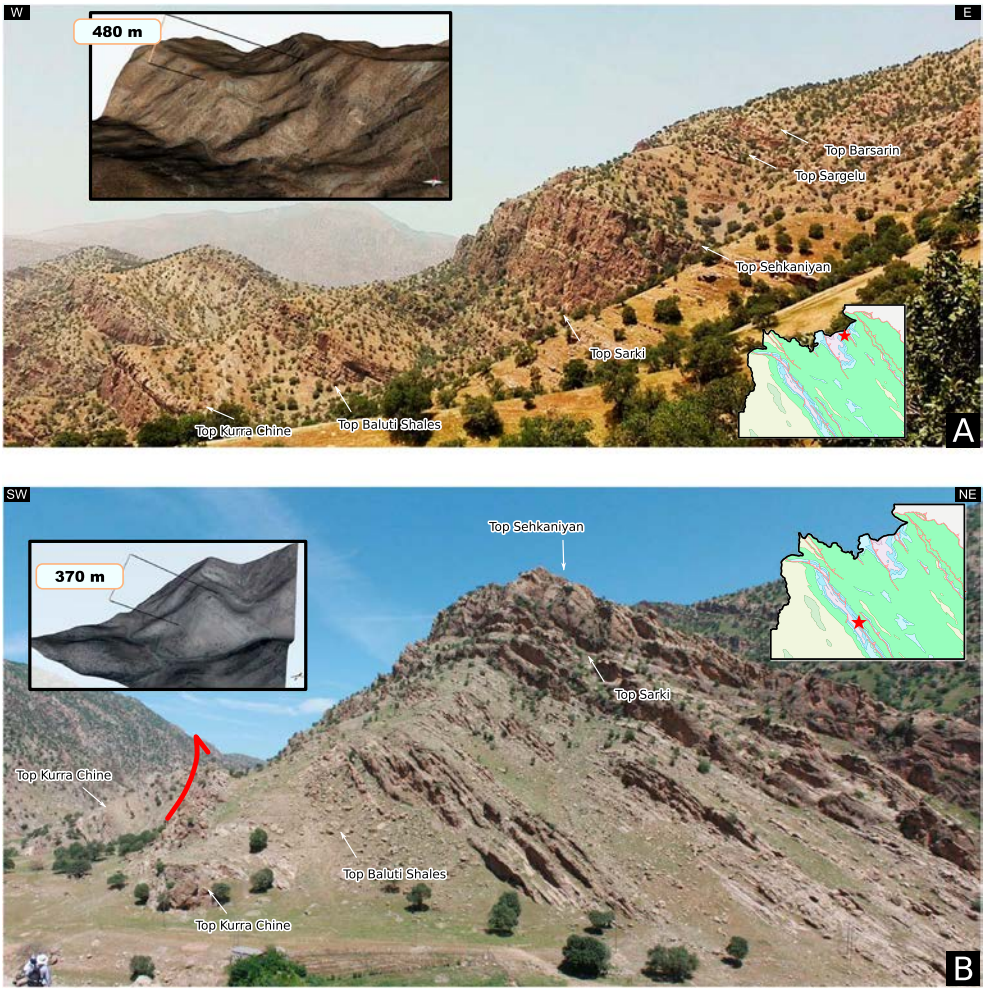

Figure 4. Triassic to Cretaceous units. Panoramic views of the Kurra Chine to Garau Fms. succession (a) and Kurra Chine to Sehkaniyan Fms. succession (b). The two insets show the location and the 3-D models of the exposures (where the computed thickness of the Baluti Shales to Sehkaniyan Fms. interval is provided).

Sargelu Fm. marks an important change from shallow-water carbonate platform environment to a deep-water basin environment. The thickness of the Sargelu Fm. in the area ranges from a few tens of meters up to 100 m. On top of the Sargelu Fm., the Callovian-Kimmeridgian Naokelekan Fm. includes a package of about 10 m of thin-bedded pelagic limestones sandwiched between two beds of oil shales. The overlying Kimmeridgian-Tithonian Barsarin Fm. consists of about 20 m of stromatolitic dolostones and dolomitic breccias, resulting from solution-collapse of evaporites. As it occurs for the Baluti Shales to Sehkaniyan Fms. package, also, the Sargelu-Naokelekan-Barsarin package is characterized by lateral thickness variations. However, these occur across shorter distances, as shown in Figure 5 and further detailed in the next sections. The Barsarin Fm. is overlain by the Lower Cretaceous Garau Fm., which is made up of deep-water well-bedded marls, shales, and limestones containing abundant radiolarians in the basal interval, and planktic foraminifers and radiolarians in the middle and upper parts. Calcarenitic beds occur at different stratigraphic levels. In the northeasternmost outcrops, the Garau Fm. is characterized by the occurrence of meter-thick packages entirely made of cherty layers, evidencing a deeper-water facies, transitional between the *normal* Garau Fm. and the sedimentary rocks of the Radiolarite Basin to the NE. The overlying Sarvak and Ilam Fms. in the northern portion of the Lurestan are mostly made of well-bedded pelagic limestones (Koop & Stoneley, 1982). In the study area, the stratigraphic boundaries between the Garau, Sarvak, and Ilam Fms. entail only subtle and gradual lithological changes and are not yet mapped correctly. For this reason, these formations are lumped together in the geological map of Figure 2. The cumulative apparent thickness of these three formations is highly variable, spanning from less than 400 m up to 2 km (Figure 6). Part of this

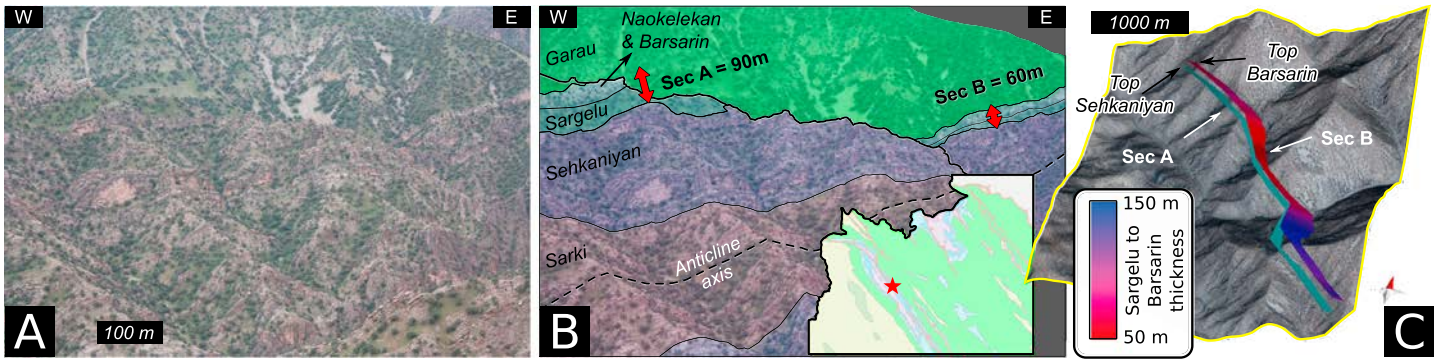

Figure 5. Thickness variation in Jurassic units. (a) Photograph and (b) line drawing of a panoramic view showing the variable thickness of the Sargelu-Naokelekan-Barsarin interval. (c) 3-D model of layers showing the top of the Sehkaniyan and of the Barsarin Fms., showing the thickness variation within the Sargelu-Naokelekan-Barsarin interval.

thickness variation is related to the effect of minor thrusting and folding. However, the present thickness distribution is mostly the result of preorogenic thickness variations in the order of many hundreds of meters, as previously remarked by other authors (e.g., Bordenave & Hegre, 2010; Sadeghi & Yassaghi, 2016). On top of the Ilam Fm., the Upper Cretaceous to lower Paleocene Gurpi Fm. is made of a thick sequence of gray marls with thin intercalations of marly limestones. This is the youngest formation cropping out in the inner-folded area, where we carried out our structural observations. The detailed description of Cenozoic rocks of the area to the SW of the study area can be found in Casciello et al. (2009), Vergés et al. (2011), and Saura et al. (2011), and they are not provided in this work.

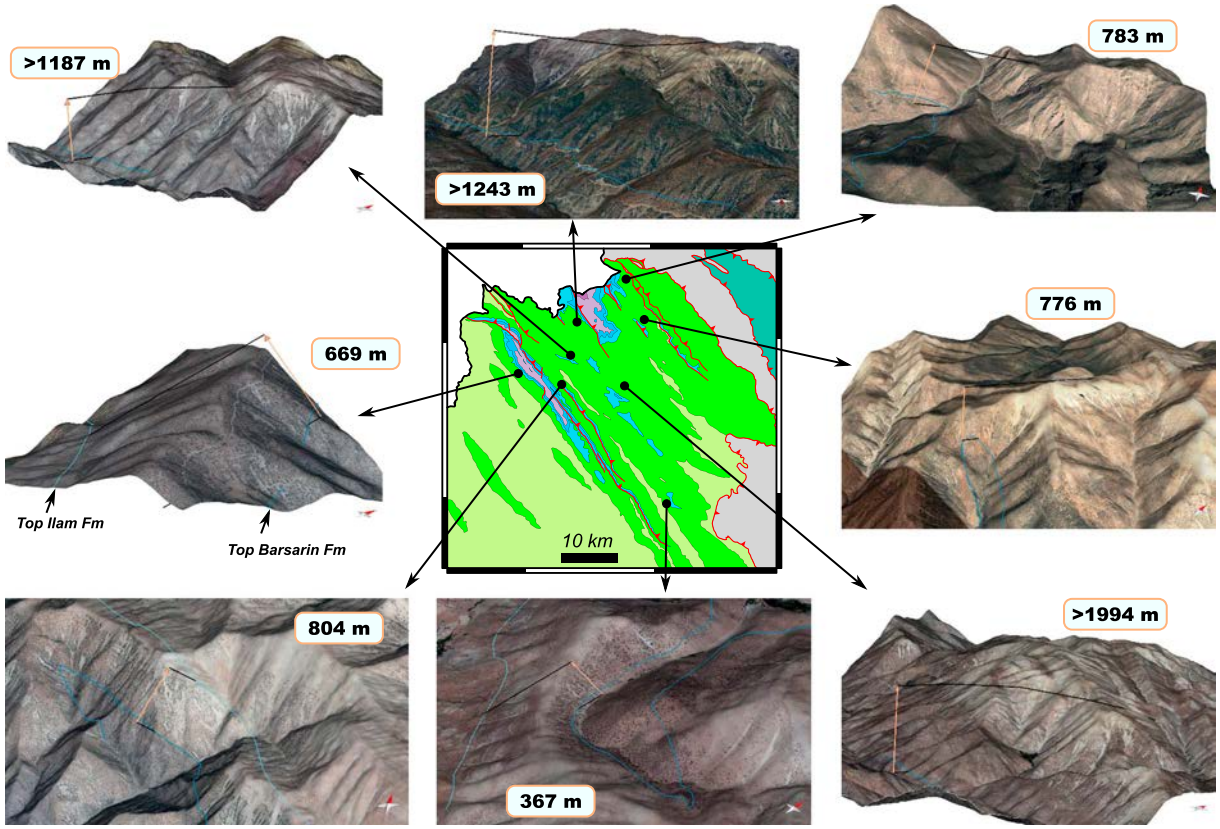

Figure 6. Thickness variation in the Cretaceous sequence. Digital elevation model with orthophoto overlay of different sectors of the study area. The top of the Barsarin Fm. and the top of the Ilam Fm. (where exposed) are indicated for each sector, along with the computed thickness of the package comprised between such formation boundaries (including the Garau, Sarvak, and Ilam Fms.).

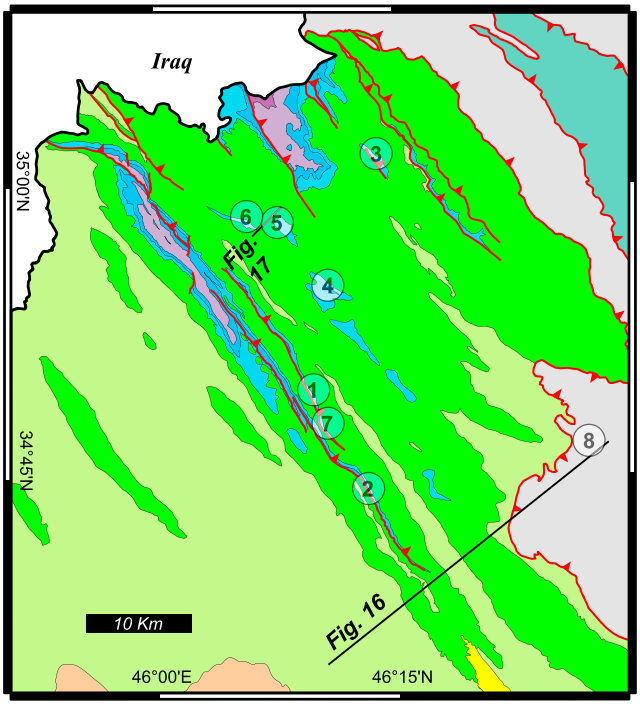

Figure 7. Map of syn-sedimentary structures. Location of the syn-sedimentary structures described in this work.

2.2. The Radiolarite Zone

The High Zagros Fault separates sedimentary rocks of the Radiolarite nappe in its hanging wall from those of the outer Arabian zone in its footwall. The deep basin succession of the Radiolarite zone is known as the *Kermanshah radiolarites* and has an age spanning from Pliensbachian to Turonian (Gharib & De Wever, 2010). It consists of an alternation of thin-bedded cherts, shales, marls, and limestones, with some thin pyroclastic levels and carbonate conglomerates and calcarenites (Abdi et al., 2014). Calciclastic inputs are recorded at different stratigraphic elevations of the multilayer; however, they are particularly abundant in the uppermost, mid-Cretaceous, portion (Jassim & Buday, 2006; Sadeghi & Yassaghi, 2016). The basement of the Radiolarite trough is currently interpreted as being represented, at least in its NE portion, by exhumed mantle (Wrobel-Daveau et al., 2010), as observed in the Harsin Basin, where the contact between cherts and peridotites is exposed.

2.3. The Bisotun Zone

To the NE, the sedimentary succession of the Radiolarite nappe lies in the footwall of the Bisotun thrust, which transported in its hanging wall about 2–3-km-thick succession of the Bisotun carbonates (e.g., Braud, 1987). These sedimentary rocks include Upper Triassic to Lower Cretaceous shallow-water carbonates (mostly limestones), locally capped by Upper Cretaceous radiolarites and limestones (Braud, 1987; Ricou et al., 1977; Wrobel-Daveau et al., 2010). The absence of shales and dolostones, as well as the absence of Jurassic and Lower Cretaceous deep-water facies, makes the stratigraphic succession of the Bisotun zone remarkably different from that of the Arabian margin (Figure 2b).

3. Evidence of Extensional Tectonics

In this section we illustrate several sites (Figure 7) showing field evidence of syn-sedimentary extensional deformation in the outer Arabian margin and in the Radiolarite nappe, along with fault data collected at the mesoscale in the preextensional to syn-extensional stratigraphic succession of the Arabian margin. Subsequently, we present a seismic cross section illustrating the positive inversion of a Jurassic graben structure.

3.1. Field Data

Extensional structures, such as faults and joints, are widespread in the Arabian zone and in the Radiolarite nappe. In the following, we first present features evidencing an indisputable syn-sedimentary character. Later, we provide data about all of the extensional faults collected in the Triassic to Middle Jurassic portion of the Arabian multilayer. As the main purpose of this work is to shed light onto the Triassic and Jurassic tectonics of the area, the few syn-sedimentary structures recognized in the Upper Cretaceous succession are not reported.

For many of the syn-sedimentary structures, in order to ease their documentation, virtual outcrop models were built by means of multiview photogrammetry (Bistacchi et al., 2015; Tavani et al., 2014; Verhoeven, 2011). Orthographic views of these models looking through directions of interest are provided, representing distortion-free and properly oriented natural cross sections of the related outcrops, on which quantitative analysis are carried out (Corradetti et al., 2017; Tavani et al., 2016). A first remarkable observation, for determining the timing of the extensional deformation in the study area, is the lack of evidence for syn-sedimentary faulting or extensional folding in the exposures of the Triassic Geli Khana and Kurra Chine Fms. These exposures include some kilometer-wide, poorly vegetated cliffs, like that shown in Figure 3. Along these well-exposed cliffs, no syn-sedimentary extensional structures have been detected. The Baluti Shales Fm. also displays no syn-sedimentary structures at the outcrop scale. The oldest rocks of the area

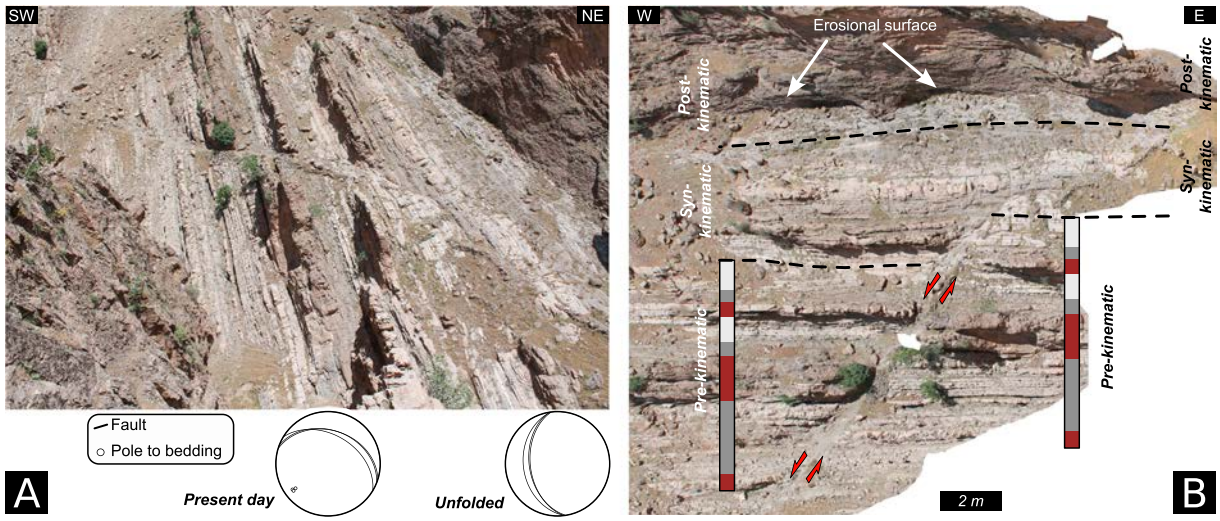

Figure 8. Syn-sedimentary fault in the Sarki Fm. Syn-sedimentary extensional fault in the Sarki Fm. at site 1 (latitude 34.8612°; longitude 46.1362°). (a) Photograph with stereoplots of data in the present day orientation and after bedding dip removal. (b) Interpreted orthorectified frontal view of a virtual outcrop model made by means of multiview photogrammetry (with bed restored to the horizontal) and structural interpretation.

showing evidence of syn-sedimentary tectonics are Lower Jurassic in age and belong to the upper portion of the Sarki Fm.

3.1.1. Sarki Fm.

The first syn-sedimentary structure described in this work is located in the southwestern portion of the study area, close to the Kezi village, in the northeastern limb of a tight anticline cored by a NE-dipping thrust fault. The hanging wall of the thrust exposes steeply dipping strata of the Sarki and Sehkaniyan Fms. A syn-sedimentary fault is hosted in dolostones and limestones of the Sarki Fm. (Figure 8a), stratigraphically located about 50 m below the boundary with the overlying Sehkaniyan Fm. The fault is NNE-dipping and, in its present orientation, displaces in a reverse sense thinly bedded dolostones and limestones, which are dipping 70° toward NE. Removing the tilting of beds leads the fault to become N-S striking and W dipping of about 50°, as seen in the stereoplot of Figure 8a. The virtual outcrop model of the fault, seen in orthographic view, is shown in Figure 8b. The orthophoto was obtained by using the fault-bedding intersection as a point of view, and it is rotated in order to set the bedding horizontal (Figure 8b). This procedure helps to highlight the prefolding architecture of the outcrop. The prekinematic package seen in Figure 8b is offset by about 2 m in a normal sense. The syn-kinematic package has a mean thickness of about 3 m in the footwall and 4 m in the hanging wall, reaching its maximum thickness of about 5 m close to the fault. The lower portion of the postkinematic package is slightly bent and displaced, thus being probably late kinematic. However, the occurrence of an erosional surface prevents any further detailed estimation of displacement and thickness variation. Along the same thrust sheet, NE-dipping limestones and dolostones of the uppermost portion of the Sarki Fm. are affected by extensional faults and by an unconformity. Some of the faults display a clear syn-sedimentary character, like the NE-dipping normal fault that bounds to the SW the graben structure illustrated in Figure 9a. The poles to extensional fault exposed in this outcrop are rather scattered, as seen in the stereoplots of Figure 9a. After bedding dip removal, they form a main cluster corresponding to faults striking NE-SW. A subordinate group of faults, including the two syn-sedimentary structures of Figure 9a, instead strike NW-SE (SW dipping in their present orientation and NE dipping after bedding dip removal). The stratigraphically lower portion of the outcrop is characterized by an erosional unconformity (Figure 9b), with strata below the unconformity dipping about 70° toward the NE. The strata above the unconformity and the unconformity itself dip toward the NE too, with a dip angle of nearly 50°. This indicates a tilting of about 20° toward the NE during the deposition of the upper portion of the Sarki Fm., coherently with the NW-SE trend of syn-sedimentary faults affecting the outcrop.

3.1.2. Sehkaniyan Fm.

As previously mentioned, the Sehkaniyan Fm. is characterized by slight thickness variations in the area. However, no major syn-sedimentary features have been recognized in the thick-bedded dolostones of this

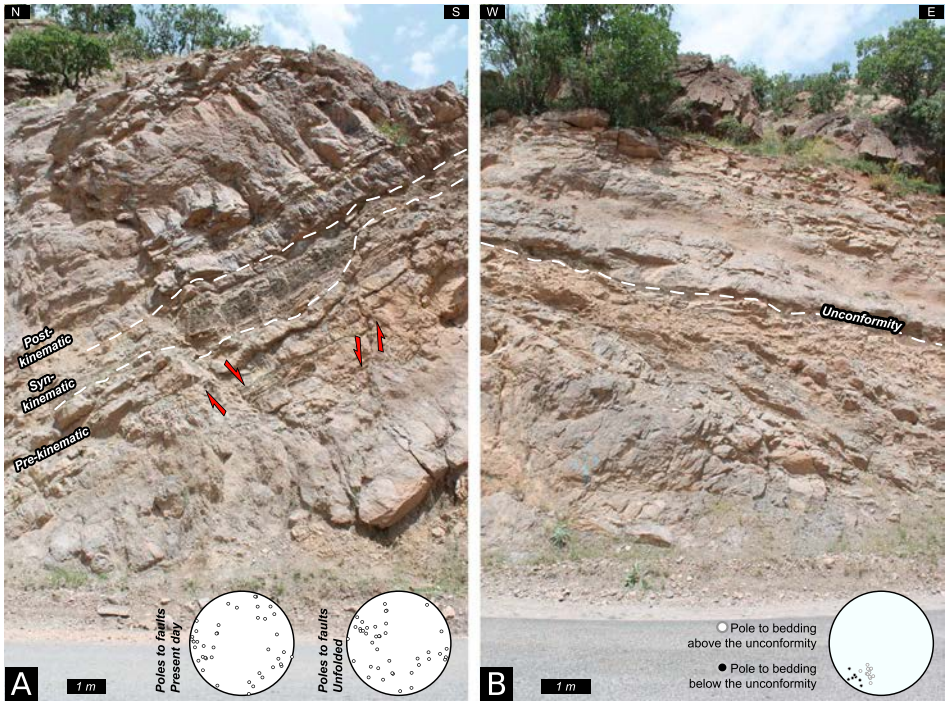

Figure 9. Syn-sedimentary structures in the Sarki Fm. Syn-sedimentary structures in the Sarki Fm. at site 2 (latitude 34.7579°; longitude 46.1995°). (a) Photograph of a syn-sedimentary graben in the Sarki Fm., with stereoplot of faults collected in the outcrop (displayed both in their present orientation and after bedding dip removal). (b) Erosional truncation occurring in the same outcrop, with stereoplot of bedding data above and below the unconformity.

formation, apart from the structure observed at site 3 and some unconformities. At site 3, meter-thick dolomitic layers are folded, with the fold axis being roughly NE-SW striking (Figure 10a). An unconformity separates the folded package from the overlying subhorizontal strata. This configuration is coherent with the occurrence of a SW-dipping normal fault active during the deposition of the Sehkaniyan Fm., with the lower—folded—package being prefaulting and the upper—subhorizontal—package being postfaulting. In some outcrops, the upper part of the Sehkaniyan Fm. is characterized by the occurrence of unconformities, like that found at site 4 and shown in Figure 10b. The observed unconformity angles do not exceed 4–5°, and due to these small values and the undulated nature of the bedding surface, it is not possible to obtain reliable measurements of bedding dip and thus of the unconformity angle.

3.1.3. Sargelu Fm.

Numerous small-scale syn-sedimentary faults occur in this formation (that illustrated in Figure 10c is located at site 4, a few meters above the unconformity of Figure 10b). In addition to these small-scale faults, major extensional structures coeval with the sedimentation of the Sargelu Fm. are observed in the study area. To the northwest of site 4, site 5 holds evidence of a first-order extensional fault developed immediately after the deposition of the Sehkaniyan Fm. The extensional fault system includes at least three faults striking NW-SE (Figures 11a and 11b) and has a cumulative offset of at least 200–300 m. The major and best-exposed fault is the northeastern one (Figures 11a–11c). This fault, separating at outcrop the Sehkaniyan Fm. in the hanging wall from the Sargelu Fm. in the footwall, dips about 70–80° toward the SW (Figure 11d). As seen in the panoramic view of Figures 11a and 11b and in the map of Figure 11c, both the northwestern and southeastern tips of the fault roughly lie along the boundary between the Sehkaniyan and Sargelu Fms., and the displacement at those tips is transferred to a fold structure. The detailed architecture of the fault at its northwestern tip is shown in Figures 11e and 11f, testifying the syn-depositional character of the fault. There, the Sehkaniyan Fm. and the first few meters of the Sargelu Fm. are faulted, whereas the middle portion of the Sargelu Fm. seals the fault. Mesoscale folds affect the hanging-wall block, in response to shortening-related buttressing. Despite such a younger overprint, thickening toward the fault of the hanging-wall formations describes a semigraben structure. Such a semigraben was filled by the

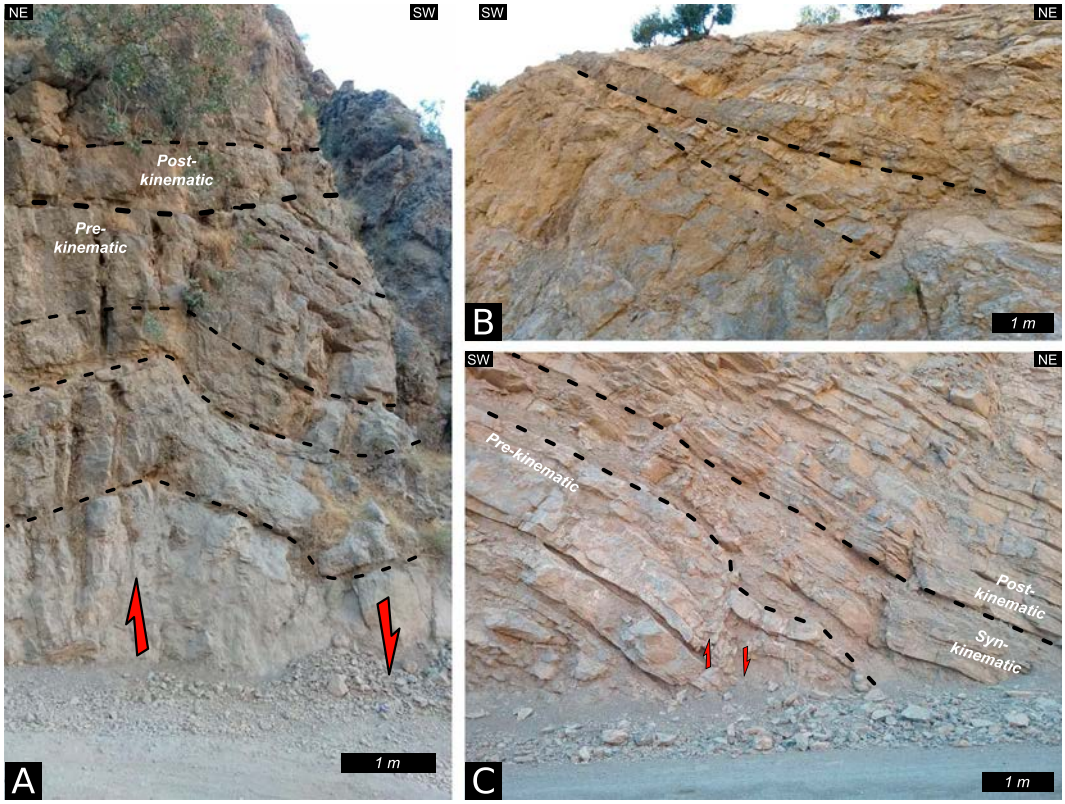

Figure 10. Syn-sedimentary structures in the Sehkaniyan and Sargelu Fms. (a) Syn-sedimentary fold in the Sehkaniyan Fm. at site 3 (latitude 35.0205°; longitude 46.2336°). (b) Unconformity at the top of the Sehkaniyan Fm. and (c) syn-sedimentary extensional fault affecting the lowermost portion of the Sargelu Fm. at site 4 (latitude 34.9087°; longitude 46.1801°).

syn-kinematic Toarcian?-Callovian Sargelu Fm. and by the postrift Naokelekan, Barsarin, and Garau Fms. that draped the hanging-wall syncline after its development.

To the SW of the previous site, syn-extensional tilting of the Sehkaniyan Fm. is documented at site 6 (Figure 12). The exposure at this site includes a SW-directed and NE-dipping low-angle thrust, with strata of the Sargelu and Naokelekan Fms. below the thrust forming a footwall syncline (Figures 12a and 12b). In the hanging wall, dolostones of the Sehkaniyan Fm. dip as the thrust and have on top the Sargelu and Naokelekan Fms. Despite the occurrence of a fold, the angular unconformity between the strata of the Sargelu-Naokelekan Fms. and those of the Sehkaniyan Fm. is well evident. The unconformity is shown also in the orthophoto extrapolated from the virtual outcrop model (Figure 12c), which was obtained by using the π axis of bedding (i.e., the SE direction) as point of view (e.g., Corradetti et al., 2017). Bedding planes in the hanging wall, both in the Naokelekan-Sargelu and Sehkaniyan Fms., are distributed along a NE-SW direction, indicating that tilting of the Sehkaniyan Fm. has occurred by a rotation about a NW-SE striking subhorizontal axis. A growth wedge in the Toarcian?-Callovian Sargelu Fm. can thus be recognized, with a tilting angle of about 22° (Figure 12c).

3.1.4. Naeokelekan and Barsarin Fms.

Within the same thrust sheet hosting sites 1 and 2, minor extensional structures occur also in the Naokelekan and Barsarin Fms. at site 7 (Figure 13). The cutoff angle of the three faults exposed in this outcrop is about 50–60°, and these faults have been tilted together with bedding during thrust-related folding. The syn-sedimentary character of the northern fault (the left one in Figure 13) is documented by the thickness change of the black shale level forming the lowermost portion of the Naokelekan Fm. The fault is sealed by well-bedded limestones of the upper portion of the same formation. An extensional fold associated with hanging-wall down-throw along the southern fault involves the upper portion of the Naokelekan Fm., with the lower portion of the Barsarin Fm. sealing the fold. The youngest fault is the central one, which is

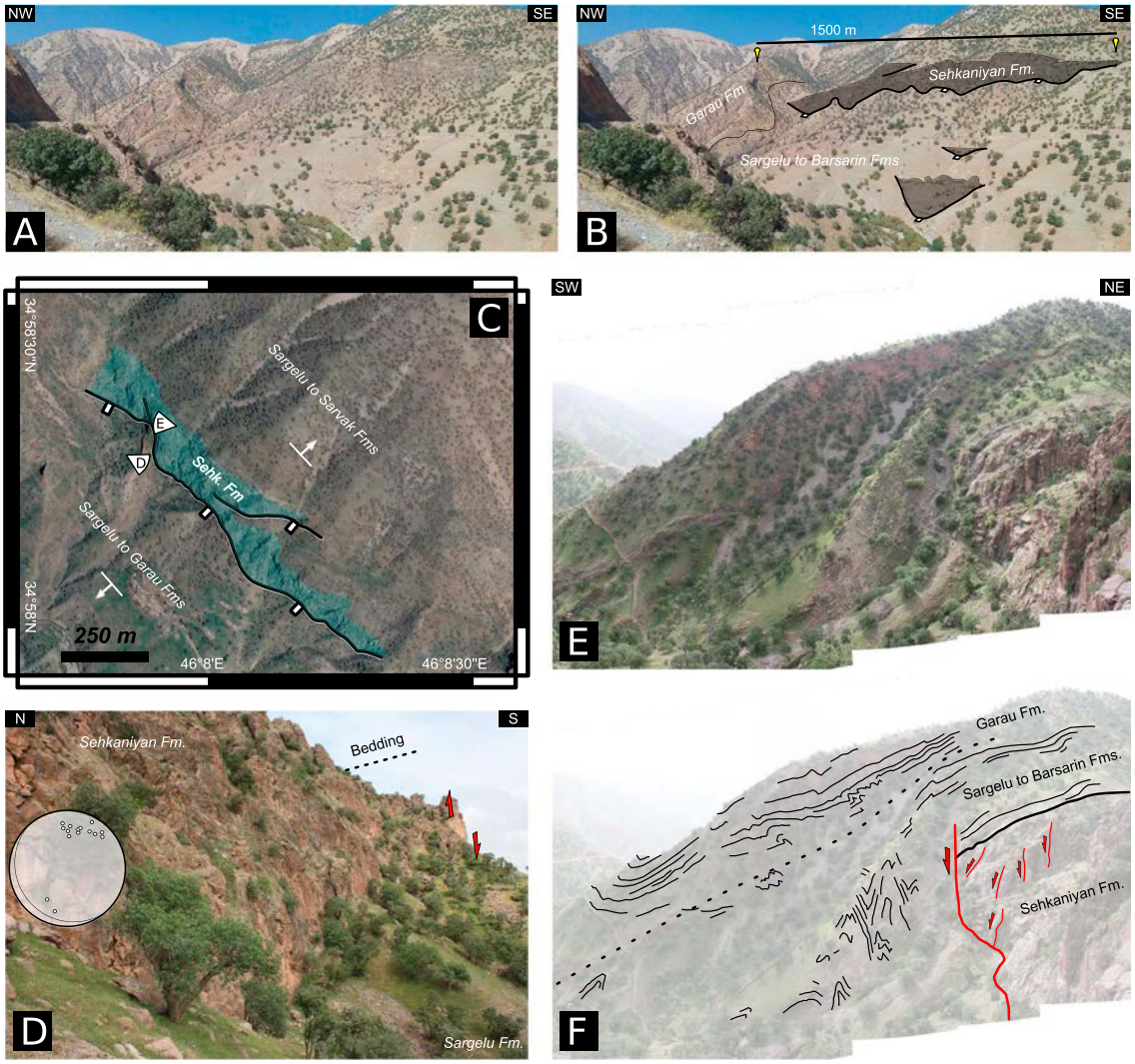

Figure 11. Syn-sedimentary fault in the Sargelu Fm. Major syn-sedimentary extensional system in the Sargelu Fm. at site 5 (latitude 34.96°; longitude 46.13°). (a) Frontal view with (b) line drawing of the extensional system, which includes three faults (the northeastern one being the largest). (c) Orthophoto with schematic structural interpretation of the area of the northeastern fault. (d) Detail of the extensional fault in (c), with stereoplot of poles to mesofaults collected in the Sehkaniyan Fm. (e) Photomosaic with (f) line drawing of the northern tip of the northeastern syn-sedimentary extensional fault, showing the uppermost portion of the Sargelu Fm. and the overlying formations fossilizing the fault and draping the hanging-wall syncline.

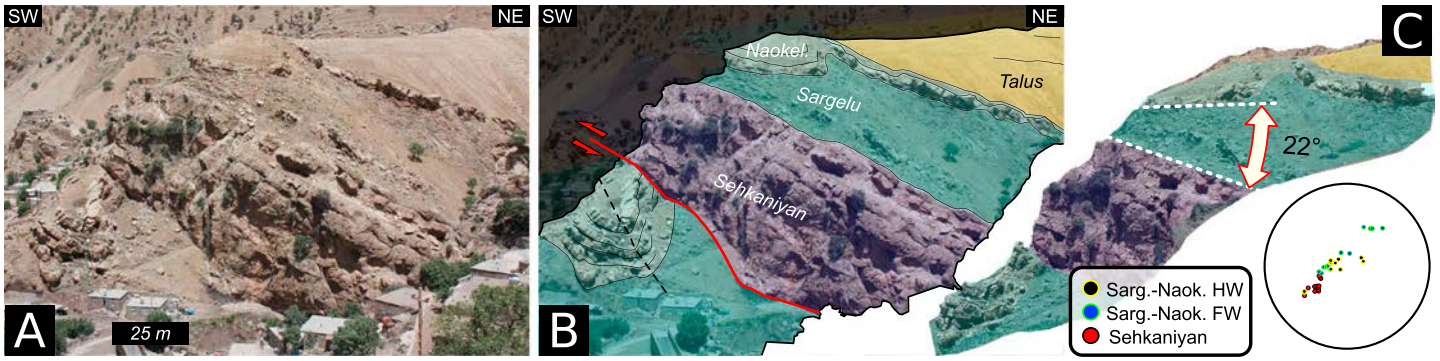

Figure 12. Extensional growth wedge in the Sargelu-Naokelekan Fms. Jurassic growth wedge in the Sargelu Fm. at site 6 (latitude 34.9683°; longitude 46.0961°). (a) Photograph and (b) line drawing of the growth wedge in the Sargelu Fm. (c) Orthophoto of the growth wedge with the wedge angle indicated and stereoplot of digitized bedding data.

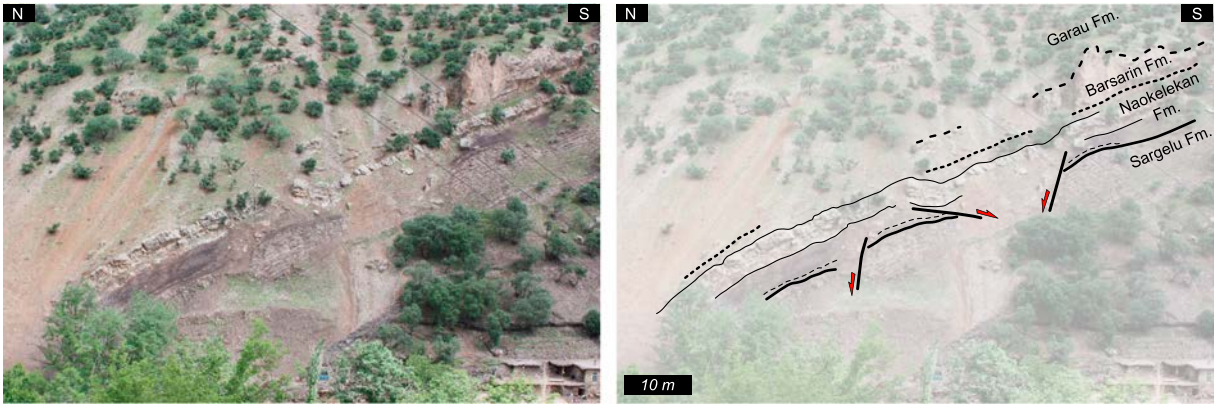

Figure 13. Syn-sedimentary faults in the Naeokelekan and Barsarin Fms. Syn-sedimentary extensional system in the Naeokelekan and Barsarin Fms. at site 7 (latitude 34.8178°; longitude 46.1663°). (a) Photograph and (b) line drawing of the syn-sedimentary normal faults. The northern fault affects the uppermost portion of the Sargelu Fm., and it is sealed by the Naokelekan Fm. The southern fault instead postdates the Naokelskan Fm. and is sealed by the Barsarin Fm.

sutured by beds of the central portion of the Barsarin Fm. or even of the Garau Fm. The three faults thus show a slightly diachronous activity, which is roughly confined within the Oxfordian to Kimmeridgian time interval.

3.1.5. Radiolarite Nappe

The last syn-sedimentary extensional structure described in this work is located within the Radiolarite nappe (site 8), in a 200-m-wide outcrop exposing ribbon cherts alternating with marls, shales, and silicified limestones. Widespread extensional structures, some of them being affected by later positive inversion, occur in the outcrop. Fault inversion is indicated by both reverse reactivation of the faults and by abundant buttressing structures, including tight folds located both in the hanging wall and in the footwall of the extensional faults. The major extensional fault of the outcrop is shown in Figures 14a and 14b. The fault

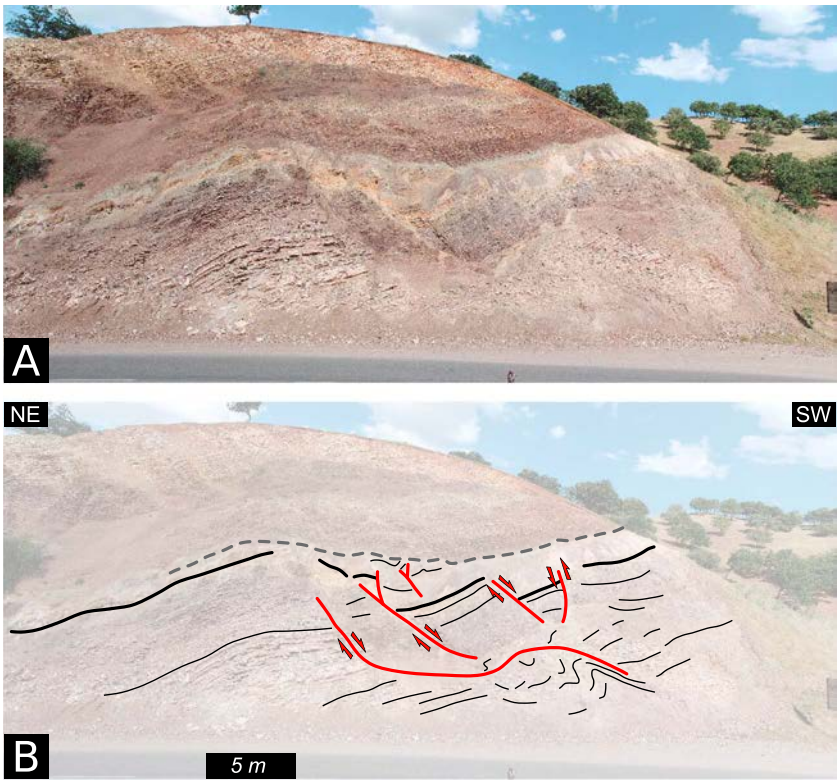

Figure 14. Syn-sedimentary faults in the Radiolarite Basin. (a) Photomosaic and (b) line drawing of a syn-sedimentary extensional fault affecting Lower Jurassic sediments of the Radiolarite Basin at site 8 (latitude 34.7781°; longitude 46.4387°).

has a ramp-flat-ramp geometry, and the southwestern segment is highly deformed by shortening-related buttressing, particularly in its footwall. However, the prekinematic, syn-kinematic, and postkinematic packages are still exceptionally well preserved in the hanging-wall block, documenting syn-depositional extensional tectonics.

The age of the levels affected by the faults, and thus of the extensional structures, has been constrained by means of nannoplankton biostratigraphy by analyzing a total of six samples. A simple smear slide was prepared for each sample by powdering a few grams of rock with distilled water and mounting the dried suspension with Norland Optical Adhesive (as described by Bown & Young, 1998). No ultrasonic cleaning and/or centrifuging were applied in order to retain the original biogenic and inorganic composition. Calcareous nannofossils were investigated with a polarizing light microscope (cross polarized, transmitted light, and quartz lamina), at 1,250X magnification. The most common taxa identified in the studied samples are illustrated in Figure 15. Calcareous nannofossil preservation is generally poor to poor/moderate, with signs of overgrowth. The nannofossil assemblage shows relatively low diversity (number of taxa) and abundance. Its composition suggests an Early Jurassic age. The most common species are *Parhabdolithus liasicus*, *Parhabdolithus robustus*, *Mitrolithus elegans*, and *Calcivascularis jansae*. Rare specimens of *Mitrolithus lenticularis*, *Crepidolithus pliensbachensis*, *Crepidolithus granulatus*, *Crepidolithus crassus*, *Schizosphaerella punctulata*, and *S. punctulata* "small", *Tubirhabdus* compare *T. patulus* have been also found. Following the stratigraphic scheme of Mattioli and Erba (1999), the presence of *M. lenticularis* and *C. crassus* (which have the first occurrence in subzone NJT3b) and the presence of *C. pliensbachensis* and *P. robustus* (which have the last occurrence at the top of subzone NJT4a) constrain the age of the studied section to the latest Sinemurian-earliest Pliensbachian, within nannofossil subzones NJT3b-NJT4a.

3.1.6. Fault Data at the Mesoscale

In addition to the syn-sedimentary features shown above, 293 meso-fault data have been collected in the Kurra Chine to Barsarin Fms. interval of the Arabian margin (Figure 16), that is, the preextensional to syn-extensional interval. Only 92 meso-faults have been measured in the Radiolarite nappe, 18 of them having slickenside striations. Due to these low numbers, fault data in the Radiolarite nappe are not shown here. Poles to meso-fault are rather scattered, being characterized in their present orientation by two main maxima corresponding to NE- and SW-dipping fault planes, respectively. The same two clusters are observed when bedding dip is restored to the horizontal, the cutoff angles of faults associated with both of them being nearly 60–70°. A total of 91 striations/shear fiber lineations has been measured, 37 of them corresponding to normal faults (i.e., normal displacement and rake comprised between 45° and 135°) in the present day orientation, becoming 47 when bedding dip is restored to the horizontal. Slickenlines and rotaxes (i.e., the slip-normal direction; Salvini & Vittori, 1982; Tavani et al., 2011) evidence two clusters for normal faults, being well evident in the unfolded analyses. The major cluster corresponds to normal faults having nearly 60° plunging and NE-SW trending slickenlines, corresponding to sub-horizontal and NW-SE-trending rotaxes. The second broad cluster instead includes normal faults having E-W to NW-SE trending and 40° to 70° plunging slickenlines, corresponding to sub-horizontal and N-S to NE-SW-trending rotaxes.

3.2. Seismic Section

In recent years, the National Iranian Oil Company has acquired a data set of near vertical seismic reflection profiles in the northwestern part of the Lurestan region, with a few of them being located in the Inner Folded Zone. Among these lines, those crossing our study area, where Jurassic and Triassic carbonates are exposed and karstified, are characterized by a remarkable noise and by poor lateral continuity of reflectors. These features make the interpretation of seismic lines not straightforward. To the SE, instead, the seismic signal becomes more coherent. The closest seismic section allowing one to shed light on the deep structure of the Inner Folded Belt is located a few tens of kilometers to the SE of our study area (Figure 7). Section 94ZHB20 runs NE-SW and crosses the High Zagros Fault and three anticlines of the Inner Folded Zone (Figure 17a). All of the anticlines along the section are cored by the Garau Fm. at the surface; however, the Jurassic Sehkaniyan Fm. is very close to the surface in the central and northeastern anticlines and is exposed along their strike a few kilometers to the NW. These three anticlines are separated by two synclines cored by marls and shales of the Upper Cretaceous Gurpi Fm., which are also exposed to the NE and SW of the fold system. The boundary between the thick-bedded dolostone of the Sehkanyian Fm. and the shales, marls, and thin-bedded limestones of the overlying Sargelu, Naokelekan, Barsarin, and Garau Fms. is well marked

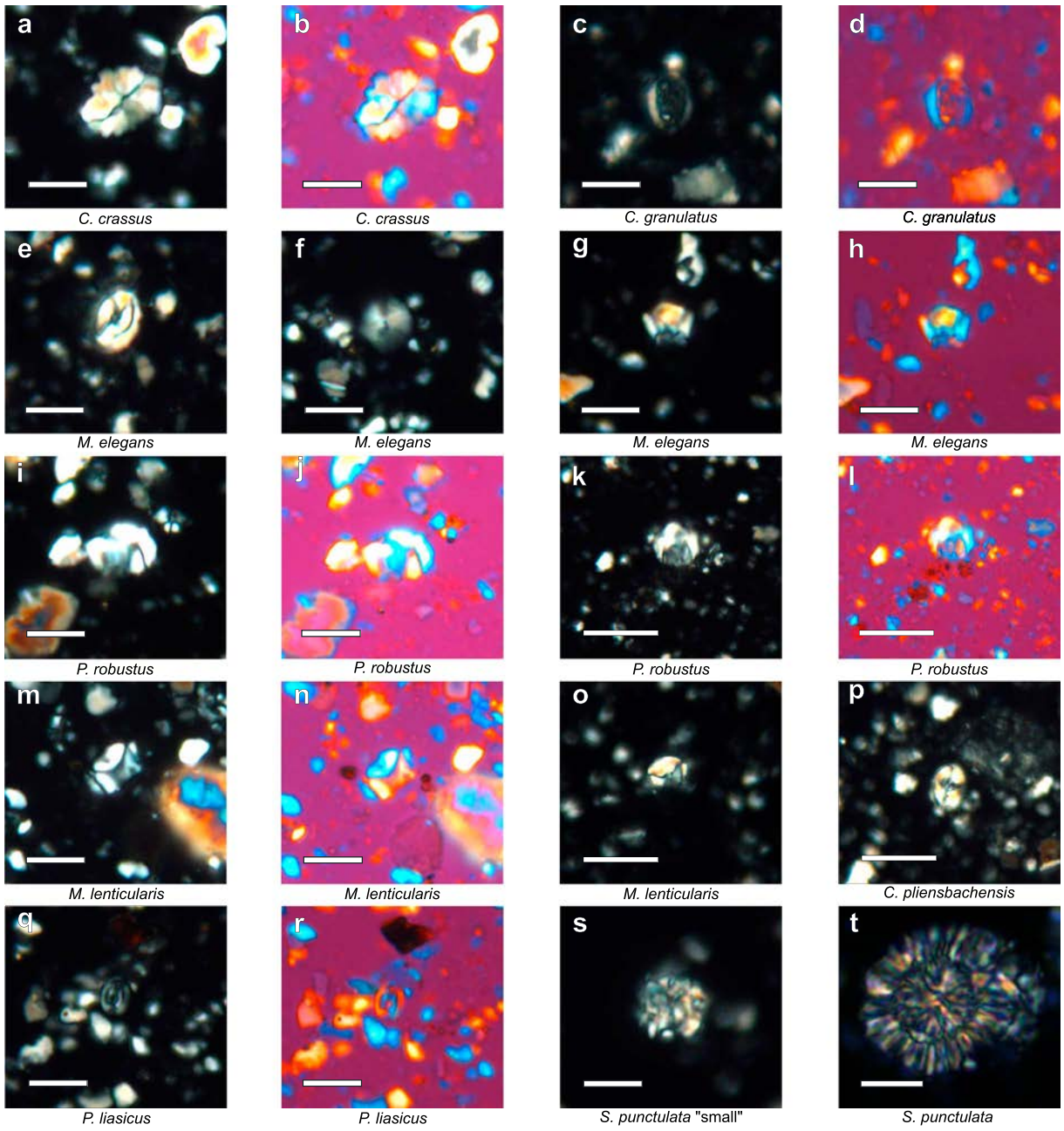

Figure 15. Main coccolith species identified in the outcrop of the Radiolarite nappe (site 8). The scale bar is 5 μm long. Pictures are taken with polarized light. (a) *Crepidolithus crassus* (cross polarized, sample 143_5); (b) *Crepidolithus crassus* (quartz lamina, sample 143_5); (c) *Crepidolithus granulatus* (cross polarized, sample 143_5); (d) *Crepidolithus granulatus* (quartz lamina, sample 143_5); (e) *Mitrolithus elegans* (cross polarized, sample 143_4); (f) *Mitrolithus elegans* (cross polarized, sample 143_4); (g) *Mitrolithus elegans* (cross polarized, sample 143_4); (h) *Mitrolithus elegans* (quartz lamina, sample 143_4); (i) *Parhabdolithus robustus* (cross polarized, sample 143_5); (j) *Parhabdolithus robustus* (quartz lamina, sample 143_5); (k) *Parhabdolithus robustus* (cross polarized, sample 143_5); (l) *Parhabdolithus robustus* (quartz lamina, sample 143_5); (m) *Mitrolithus lenticularis* (cross polarized, sample 143_5); (n) *Mitrolithus lenticularis* (quartz lamina, sample 143_5); (o) *Mitrolithus lenticularis* (cross polarized, sample 143_5); (p) *Crepidolithus pliensbachensis* (cross polarized, sample 143_5); (q) *Parhabdolithus liasicus* (cross polarized, sample 143_5); (r) *Parhabdolithus liasicus* (quartz lamina, sample 143_5); (s) *Schizosphaerella punctulata* "small" (cross polarized, sample 143_4); (t) *Schizosphaerella punctulata* "small" (quartz lamina, sample 143_5).

in the seismic profile (Figures 17b and 17c). The boundary between the limestones of the Ilam Fm. and the marls and shales of the Gurpi Fm. is recognizable as well. Using also the robust constraints of surface geology, we were able to map these two horizons in the seismic line of Figure 17, where we also marked some reflectors attributable to the Triassic and Paleozoic sedimentary succession, to ease the structural

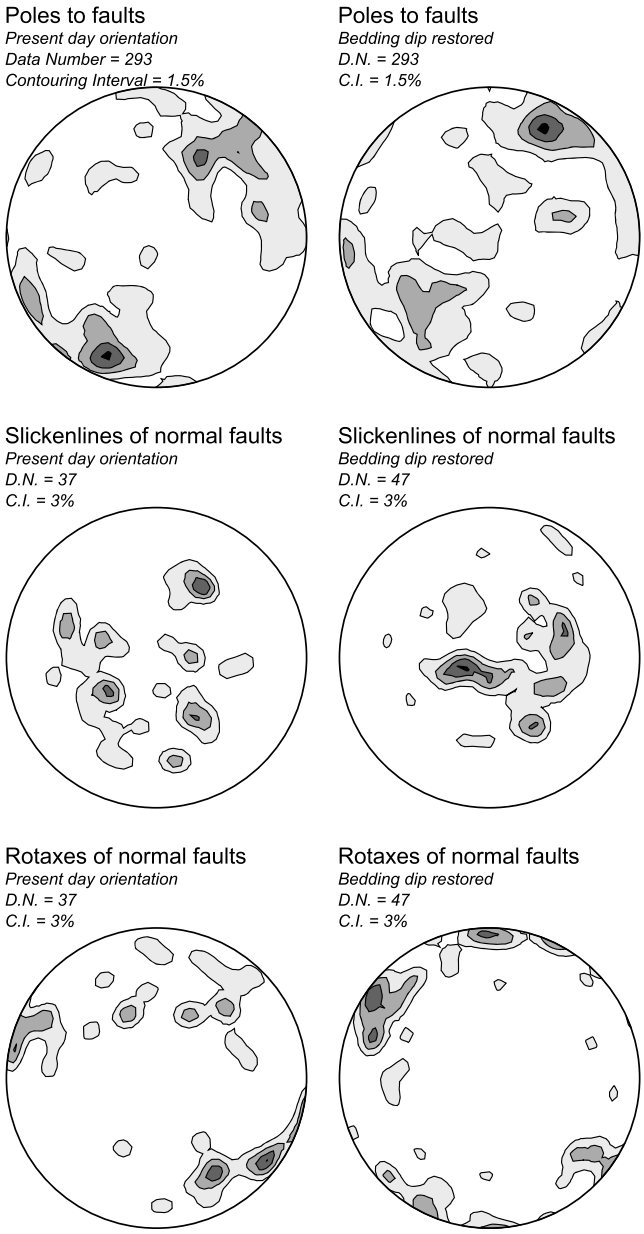

Figure 16. Meso-fault data in the Kurra Chine to Naokelekan Fms. Cumulative density contour of poles to faults and of both striations and rotaxes (i.e., slip-normal) of normal faults collected in the prerift to syn-rift sedimentary successions of the Arabian domain. Data are displayed both in the present-day orientation and after bedding dip removal.

interpretation. Southwest of the High Zagros fault, the seismic profile shows a zone of folded reflectors flanked to the SW and NE by SW- and NE-dipping reflectors, respectively, forming two ~10-km-wide monoclines. Layers within the folded system show geometries (anticlines and synclines) consistent with those observed at the surface. The elevation of the Sehkanyian Fm. below the two synclines of the folded system is lower than that at the borders of the two external monoclines. The vertical and lateral continuity of reflectors within the bounding monoclines indicates that the folded system is underlain to the SW and NE by steeply dipping faults, dipping to the NE and SW, respectively. These features indisputably point to a pop-up structure produced by the reactivation and positive inversion of a graben structure.

4. Discussion

The geological structures exposed in the field and reconstructed in the seismic section indicate that, during the Jurassic, an extensional pulse occurred in the northwestern portion of the Lurestan area of the Zagros. Syn-sedimentary faults, unconformities, and growth geometries are documented in a large portion of the analyzed sedimentary succession, starting from the uppermost (Lower Jurassic) portion of the Sarki Fm., up to the Upper Jurassic Barsarin Fm. Syn-sedimentary faults are mostly NW-SE striking, while unconformities and growth geometries indicate a rotation of layers about a NW-SE-oriented horizontal axis. The meso-faults measured in the prerift to syn-rift portion of the multilayer are NW-SE striking too (although there is no guarantee that all of them have developed during Jurassic extension), and they display cutoff angles of nearly 60°, with the striations of normal faults dominantly indicating NE-SW extension. Kilometer-long, positively inverted, NW-SE striking normal faults occurring in the Triassic and Early Jurassic stratigraphic succession of the area have been also documented by Tavani et al. (2018). All of these data are consistent with a regionally NE-SW-oriented stretching during the Early and Middle Jurassic. This extension direction is slightly oblique to the NNE-SSW direction of extension documented by Navabpour et al. (2011) for the same time interval in the Radiolarite basin. However, it is worth noting that the intensely folded, thinly bedded sediments of the Radiolarite zone lie in the hanging wall of a regional thrust having probably more than 10 km of displacement (e.g., Sadeghi & Yassaghi, 2016; Tavani et al., 2018; Vergés et al., 2011), and therefore, syn-thrusting vertical axis rotations cannot be ruled out.

Information about the regional relevance of the extensional structures documented in the Lurestan is provided by field data and seismic interpretation provided in this work and by facies maps available for the area (e.g., Barrier & Vrielynck, 2008; Koop & Stoneley, 1982; M. A. Ziegler, 2001), which are later illustrated. The major syn-sedimentary structures documented here, that is, the main faults of sites 5 and 6 (Figures 11 and 12), are late Early Jurassic to Middle Jurassic in age. These structures developed synchronously with the deposition of the Sargelu Fm., whose sedimentary evolution records the Toarcian?-Aalenian drowning of the long-lived Triassic-Jurassic carbonate platform and the onset of deep-water conditions. This indicates a tectonically controlled drowning and thus testifies the regional significance of the documented extensional pulse. Furthermore, the displacement of the major Early Jurassic fault observed at site 5 is in the order of 100 m. This fault is NW-SE striking and SW dipping, and its surface is exposed for at least 1 km, being covered by more recent units both to the NW and SW. Published data on maximum displacement versus length of extensional faults (e.g., Cowie & Scholz, 1992; Kim & Sanderson, 2005) indicate that such a fault could have a map size of a few

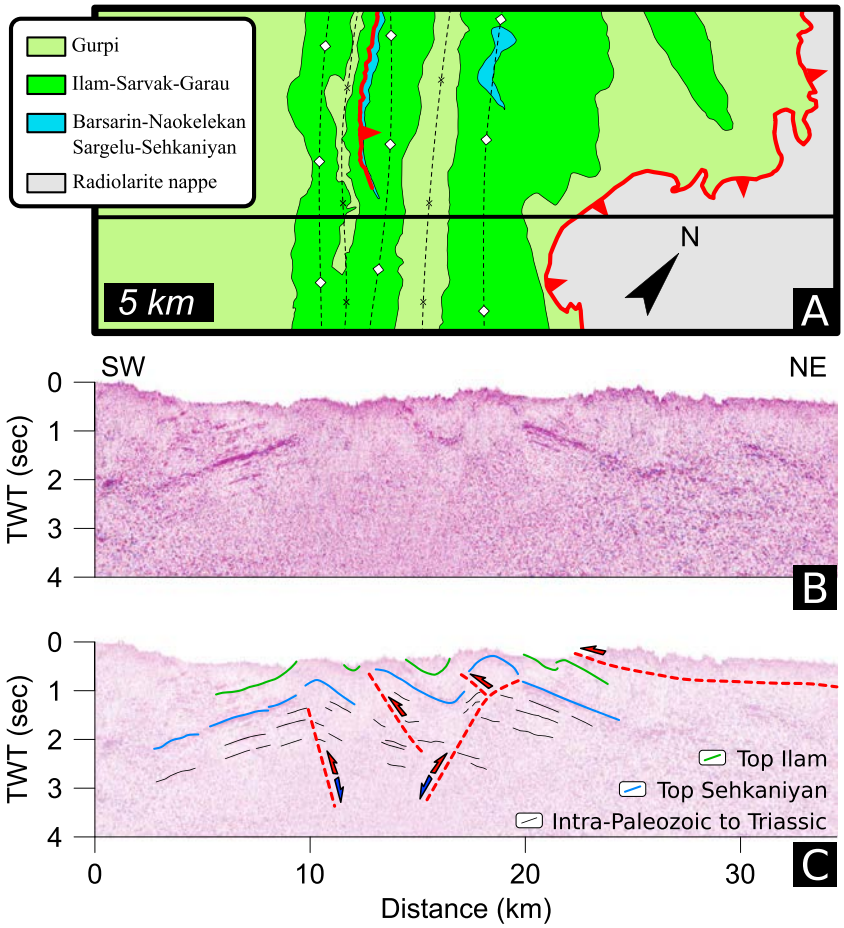

Figure 17. Seismic section showing positive inversion of an inherited graben structure. (a) Geological map in the area surrounding the section trace indicated. (b) Seismic section (TWT = two-way travel). (c) Seismic section with interpretation.

tens of kilometers. The southeastern along-strike prolongation of this fault exactly matches with the SW-dipping fault bounding to the NE the inverted graben of Figure 17, which allowed us to interpret the extensional system of site 5 and the fault located at the northern boundary of the folded system shown in Figure 17 as belonging to the same fault system. The positively inverted graben of Figure 17 is thus probably Early Jurassic in age. Such an inference is supported by the geological cross section of Figure 18 a, which covers the NE part of the graben system in its northwestern portion. The cross section strikes SW-NE, and it is built by projecting, perpendicularly to the section, data from sites 5 and 6, which are less than 5 km apart. Despite the lack of Lower and Middle Jurassic rocks in the central portion of the section, it is evident that the extensional fault of site 5 and the growth wedge of site 6 form part of the same semigraben structure, as illustrated in Figure 18b, which schematically shows the prethrusting configuration of the section. It is worth mentioning the apparent discrepancies between the estimated displacement of the extensional faults and thickness variations observed in the syn-kinematic Sargelu Fm. Our data show that the total thickness of the Sargelu, Naokelekan, and Barsarin Fms. ranges from less than 50 m up to 150 m (Figures 5, 11, and 12), with a maximum thickness difference of about 100 m. Conversely, the inferred cumulative displacement of extensional faults forming the graben is at least three times greater. Such an apparent disagreement between structures and stratigraphy is related with the deep-water depositional environment of the syn-kinematic infill. The Sargelu, Naokelekan, and Barsarin Fms. have essentially draped over faulted blocks, without leveling the paleo-bathymetry, as schematically illustrated in Figure 18b. During the interval encompassing the deposition of these three formations, the basin was underfilled, due to the very low sedimentation rate, that is, 150 m in 30 Ma. Bathymetric highs and troughs were thus still present during the Cretaceous. This is in agreement with the observation that

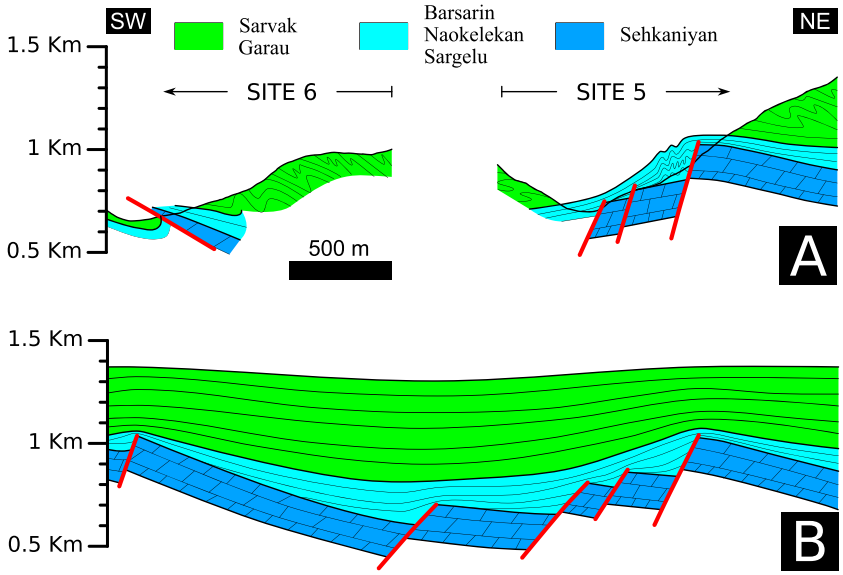

Figure 18. Geological cross section across a Jurassic semigraben. (a) NE-SW-oriented geological cross section obtained by projecting data from sites 5 and 6. (b) Scheme showing the preshortening architecture of the section.

the cumulative thickness of the postrift Garau, Sarvak, and Ilam Fms., filling the residual paleo-bathimetry, displays lateral variations in the order of hundreds of meters.

Our findings, including macrostructural and meso-structural data clearly pointing to a NE-SE direction of horizontal maximum extension, provide a key to the understanding of the occurrence of Mesozoic deep-water basins developing within the dominantly shallow water to continental settings of the Arabian Margin (Bordenave & Hegre, 2010; Koop & Stoneley, 1982; van Buchem et al., 2010). Facies distribution in the Arabian Plate (Figure 19; e.g., Barrier & Vrielynck, 2008; Koop & Stoneley, 1982; M. A. Ziegler, 2001) shows continental to shallow-water depositional environments in the large time interval spanning from the Late Permian to the Early Jurassic. With the only exception of the Hawasina Basin in the Oman area to the SE, no deep-water environments are reported during this period. A major change occurred during the Early Jurassic, with the development of two deep-water radiolarite basins, that is, the Kermanshah Radiolarite and Pichakun basins (Figure 19). Later, at the transition between the Early and the Middle Jurassic, the Sargelu and Naokelekan deep-water formations were deposited in the NW-SE elongated, so-called Sargelu Basin (Koop & Stoneley, 1982) that, according to many authors, was a tectonically controlled intrashelf basin (e.g., Alsharhan, 2014). This basin persisted until the Cretaceous, being known as the Garau Basin (Jassim & Goff, 2006; van Buchem et al., 2010; Figure 19). We have shown that the drowning of the Sehkaniyan carbonate platform during the Toarcian?-Aalenian and the onset of deep-water conditions in the Sargelu Basin were accompanied by a remarkable extensional tectonic activity. This confirms the idea of Alsharhan (2014) and allows us to interpret the Middle Jurassic to Early Cretaceous basins of the Arabian Margin as developed in response to Early-Middle Jurassic extensional tectonics. As discussed before, we have inferred a NE-SW-oriented extension, which is consistent with the NW-SE elongation of the Sargelu and Garau basins. In this work, we have also documented syn-sedimentary extensional tectonics in the latest Sinemurian-earliest Pliensbachian sedimentary rocks of the Kermanshah Radiolarite Basin (Figures 14 and 15). To date, no remarkably older deep-water sediments have been found in the Kermanshah Radiolarite Basin, indicating that the documented Sinemurian-Pliensbachian extension and the formation of the Kermanshah Radiolarite Basin were coeval processes. The Toarcian?-Aalenian drowning of the Early Jurassic carbonate platform and the Sinemurian-Pliensbachian development of the Radiolarite Basin are thus only very slightly delayed and can be framed within the same extensional event, with the Kermanshah Radiolarite Basin forming the distal portion of the Sargelu and Garau basins (Figure 19). This is further supported by the occurrence of a deeper-water facies of the Garau Fm. in the northeastern portion of the study area, transitional between the normal Garau Fm. and the sedimentary rocks of the Kermanshah Radiolarite Basin. Mantle exhumation during the development of the Kermanshah Radiolarite Basin

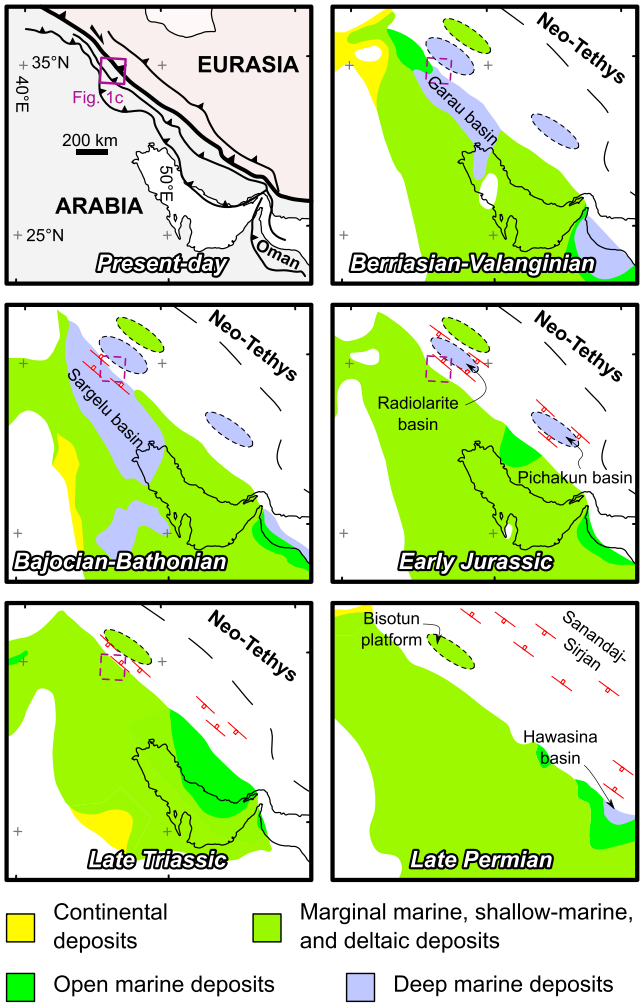

Figure 19. Paleofacies maps of the Arabian margin. Simplified paleofacies maps of the Arabian Plate (modified from Koop & Stoneley, 1982; M. A. Ziegler, 2001; Barrier & Vrielynck, 2008).

(Wrobel-Daveau et al., 2010) further emphasizes the geodynamic importance of the illustrated extensional pulse. Thus, (i) Late Triassic differentiation between the Bisotun block and the Arabian margin, (ii) Sinemurian to Pliensbachian development of the Kermanshah Radiolarite Basin, and (iii) Toarcian?-Aalenian extensional faulting in the Arabian margin are in our view steps of the same rifting process. Such an about 40–50 Myr long-time lapse is in fact largely below the average duration of the rifting process (P. A. Ziegler & Cloetingh, 2004). The fact that the younger (Toarcian?-Aalenian) structures developed in the Arabian proximal domain, rather than in the distal domains facing the ocean to the NE, points to an out-of-sequence organization of the faulting sequence. This is nowadays a widely recognized style of deformation in rifted domains (e.g., Gillard et al., 2016).

Our work points to the occurrence of two phases of rifting at the northern margin of Gondwana. During the first, Permo-Triassic phase, the Arabian Margin of the Gondwana continent was separated from the Sanandaj-Sirjan and the Central Iranian blocks to the NE by the opening of the Neo-Tethys (e.g., Berberian & King, 1981; Ghasemi & Talbot, 2006; Koop & Stoneley, 1982; Robertson, 2007; Saccani et al., 2013; Figure 19). The two conjugate neo-Tethyan passive margins were subsequently drifted away some thousands of kilometers (e.g., Muttoni et al., 2009; Stampfli & Borel, 2002). This first phase has mostly a tectono-magmatic evidence in the Zagros mountains (e.g., Ghasemi & Talbot, 2006; Saccani et al., 2013). During Permo-Triassic rifting, indeed, about 2 km of continental to shallow-marine sediments were deposited in the Arabian margin (Alavi, 2004; Bordenave, 2008; Szabo & Kheradpir, 1978), with only a few documented evidences of syn-tectonic geometries (e.g., Sepehr & Cosgrove, 2004). Permo-Triassic deep-water sediments that should have been interposed between the ocean and the inner portion of the passive margin are presently preserved only in a small area in the Oman region (Figure 19; i.e., the Hawasina Basin; Béchennec et al., 1990; De Wever et al., 1988). This indicates that the outer portions of the Permo-Triassic Arabian paleo-margin were located much to the NE of the present day position of the Zagros Belt (Figure 19). As documented here, renewed extension along the Arabian margin of Neo-Tethys occurred in the Early-Middle Jurassic, as recorded by (i) the development of the Kermanshah Radiolarite Basin and (ii) the drowning on the long-lived Permian-Early Jurassic carbonate platform domain. The lack of Triassic radiolarites in the deep-water basins of the Zagros Belt, that is, the Kermanshah Radiolarite Basin of Lurestan (Gharib & De Wever, 2010) and the Pichakun Basin some hundreds of kilometers to the SE (Robin et al., 2010; Figure 19), indicates that the two-step rifting is not a local feature of the Lurestan area. On the contrary, Jurassic extension probably affected the entire portion of the Arabian Margin presently incorporated into the Zagros Belt.

A multistep rifting event, encompassing the Permian-Jurassic interval, is also recognized immediately to the west of the Arabian paleo-margin, in the Levant Basin of the eastern Mediterranean area (e.g., Gardosh et al., 2010; Garfunkel, 2004; Garfunkel & Derin, 1984; Figure 20). The Levant Basin area is a remnant of the Jurassic junction between two segments of the Neo-Tethys: an eastern one, facing the northern margin of the Arabian platform (which includes the study area of this work), and a western one, presently occupying the eastern Mediterranean area (e.g., Sengör & Yilmaz, 1981). Opening of the Levant basin occurred in a time interval spanning from the Permian to the Early Jurassic (e.g., Gardosh et al., 2010), in response to the separation of the northern African Margin to the south from a crustal block to the north. This latter included, among the others, the Taurus and Gavrovo-Tripoliza platforms (e.g. Frizon de Lamotte et al., 2011; Sengör, 1979). At a first glance, this northern block was in continuity with the Sanandaj-Sirjan block of Iran, in the sense that these domains were forming the northern paleo-margin of the ocean located to the north of

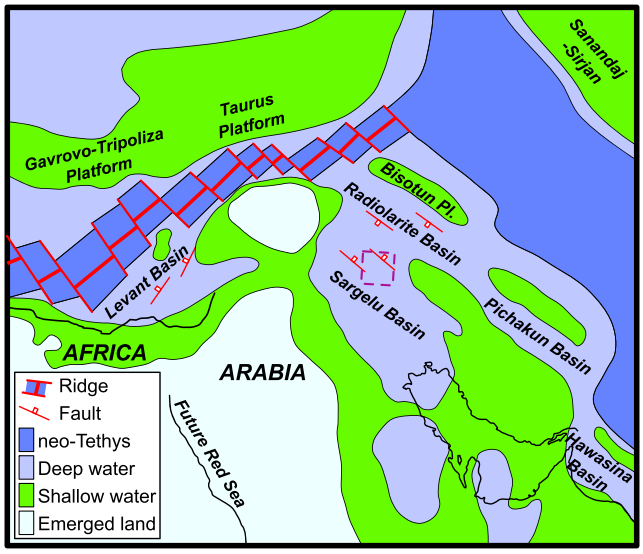

Figure 20. Paleotectonic map of Arabia and western Mediterranean area for Callovian times, modified after Barrier and Vrielynck (2008) and Frizon de Lamotte et al. (2011).

the Jurassic Arabian-African margin (e.g., Robertson, 2007; Saccani et al., 2013). The link between these blocks and, more generally, the connection between the eastern and western arms of the neo-Tethys are not straightforward. The Arabian margin is shifted northward with respect to the North African margin, and the NNE-SSW trend of the Levant basin has suggested that this originated as a Permo-Triassic transfer system linking the two arms of the Neo-Tethyan ocean (e.g., Stampfli & Borel, 2002), that is, the eastern one located to the north of the Arabian margin and the western one located to the north of the African margin (Figure 20). On the other hand, the documented N-S trend of Triassic and Jurassic extensional faults within the Levant basin (e.g., Garfunkel, 2004) is in contrast with the latter geodynamic interpretation, as it indicates E-W to WNW-ESE extension and spreading in the western arm of the Neo-Tethys until the Middle Jurassic (e.g., Frizon de Lamotte et al., 2011; Figure 20). E-W to ESE-WNW spreading in the western Neo-Tethys and coeval NE-SW extension at the southern margin of the eastern neo-Tethys (i.e., within the Arabian margin, as documented here) suggest that these two domains cannot be simply considered as two ocean arms connected by a transform system. Rather, a more complex scenario should be invoked for the Early Jurassic time, such as the triple junction suggested by Garfunkel (1998).

5. Conclusions

Structural and stratigraphic features of the Mesozoic sedimentary successions of the Lurestan region of the Arabian passive margin provide a comprehensive record of Jurassic extensional tectonics. Extensional deformation spanning from the Early to the Late Jurassic is testified by syn-sedimentary faults, block tilting, and unconformities and by facies and thickness changes. These features consistently indicate that extensional deformation reached its peak at the transition from the Early to the Middle Jurassic, when faulting caused drowning of large areas of the Triassic to Early Jurassic carbonate platform of the passive margin, and the onset of deep-water environments in tectonically controlled troughs. Coherently with regional evidence, we propose that rifting and breakup of Pangea in the studied area was achieved during two stages. An early Permo-Triassic rifting stage was followed by the late Early to Middle Jurassic pulse documented in this study, which strongly shaped the passive margin.

Acknowledgments
Thoughtful and constructive reviews by Dominique Frizon de Lamotte and Eric Barrier are gratefully acknowledged. Midland Valley is thanked for providing the Move software (Academic License to the University of Naples Federico II). We acknowledge the use of imagery from the Land Atmosphere Near-real time Capability for EOS (LANCE) system, operated by the NASA/GSFC Earth Science Data and Information System (ESDIS)—https://earthdata.nasa.gov/—with funding provided by NASA/HQ. Requests for obtaining the near-vertical seismic section in Figure should be submitted to the National Iranian Oil Company. All the other data used in this work are listed in the references.

References

Abdi, A., Gharaie, M. H. M., & Bádenas, B. (2014). Internal wave deposits in Jurassic Kermanshah pelagic carbonates and radiolarites (Kermanshah area, West Iran). *Sedimentary Geology*, *314*, 47–59. https://doi.org/10.1016/j.sedgeo.2014.10.006

Agard, P., Omrani, J., Jolivet, L., & Mouthereau, F. (2005). Convergence history across Zagros (Iran): Constraints from collisional and earlier deformation. *International Journal of Earth Sciences (Geologische Rundschau)*, *94*(3), 401–419. https://doi.org/10.1007/s00531-005-0481-4

Agard, P., Omrani, J., Jolivet, L., Whitechurch, H., Vrielynck, B., Spakman, W., et al. (2011). Zagros orogeny: A subduction-dominated process. *Geological Magazine*, *148*(5–6), 692–725. https://doi.org/10.1017/S001675681100046X

Alavi, M. (1980). Tectonostratigraphic evolution of the Zagrosides of Iran. *Geology*, *8*(3), 144–149. https://doi.org/10.1130/0091-7613(1980)8<144:TEOTZO>2.0.CO;2

Alavi, M. (1991). Sedimentary and structural characteristics of the Paleo-Tethys remnants in northeastern Iran. *Geological Society of America Bulletin*, *103*(8), 983–992. https://doi.org/10.1130/0016-7606(1991)103<0983:SASCOT>2.3.CO;2

Alavi, M. (1994). Tectonics of Zagros orogenic belt of Iran, new data and interpretation. *Tectonophysics*, *229*(3–4), 211–238. https://doi.org/10.1016/0040-1951(94)90030-2

Alavi, M. (2004). Regional stratigraphy of the Zagros fold-thrust belt of Iran and its proforeland evolution. *American Journal of Science*, *304*(1), 1–20. https://doi.org/10.2475/ajs.304.1.1

Alavi, M. (2007). Structures of the Zagros fold-thrust belt in Iran. *American Journal of Science*, *307*(9), 1064–1095. https://doi.org/10.2475/09.2007.02

Alsharhan, A. S. (2014). Petroleum systems in the Middle East. *Geological Society of London, Special Publication*, *392*(1), 361–408. https://doi.org/10.1144/SP392.19

Bahroudi, A., & Koyi, H. (2003). Effect of spatial distribution of Hormuz salt on deformation style in the Zagros fold and thrust belt: An analogue modelling approach. *Journal of the Geological Society*, *160*(5), 719–733. https://doi.org/10.1144/0016-764902-135

Barrier, E., & Vrielynck, B. (Eds) (2008). *Paleotectonic maps of the Middle East: Atlas of 14 maps*. Middle East Basin Evolution (MEBE): Programme.

Béchennec, F., Le Métour, J., Rabu, D., Bourdillon-de-Grissac, C. H., De Wever, P., Beurrier, M. T., & Villey, M. (1990). The Hawasina nappes: Stratigraphy, palaeogeography and structural evolution of a fragment of the south-Tethyan passive continental margin. *Geological Society, London, Special Publications*, *49*(1), 213–223. https://doi.org/10.1144/GSL.SP.1992.049.01.14

Berberian, M. (1995). Master "blind" thrust faults hidden under the Zagros folds: Active basement tectonics and surface morphotectonics. *Tectonophysics*, *241*(3–4), 193–224. https://doi.org/10.1016/0040-1951(94)00185-C

Berberian, M., & King, G. C. P. (1981). Towards a paleogeography and tectonic evolution of Iran. *Canadian Journal of Earth Sciences*, *18*(2), 210–265. https://doi.org/10.1139/e81-019

Bistacchi, A., Balsamo, F., Storti, F., Mozafari, M., Swennen, R., Solum, J., et al. (2015). Photogrammetric digital outcrop reconstruction, visualization with textured surfaces, and three-dimensional structural analysis and modeling: Innovative methodologies applied to fault-related dolomitization (Vajont Limestone, Southern Alps, Italy). *Geosphere*, *116*, 2031–2048.

Blanc, E. P., Allen, M. B., Inger, S., & Hassani, H. (2003). Structural styles in the Zagros simple folded zone, Iran. *Journal of the Geological Society*, *160*(3), 401–412. https://doi.org/10.1144/0016-764902-110

Bordenave, M. L. (2008). The origin of the Permo-Triassic gas accumulations in the Iranian Zagros Foldbelt and contiguous offshore areas: A review of the Paleozoic petroleum system. *Journal of Petroleum Geology*, *31*(1), 3–42. https://doi.org/10.1111/j.1747-5457.2008.00405.x

Bordenave, M. L., & Hegre, J. A. (2010). Current distribution of oil and gas fields in the Zagros Fold Belt of Iran and contiguous offshore as the result of the petroleum systems. *Geological Society of London, Special Publication*, *330*(1), 291–353. https://doi.org/10.1144/SP330.14

Bown, P. R., & Young, J. R. (1998). Techniques. In P. R. Bown (Ed.), *Calcareous nannofossil biostratigraphy* (pp. 132–199). London: Chapman and Hall. https://doi.org/10.1007/978-94-011-4902-0_2

Braud, J. (1987). La suture du Zagros au niveau de Kermanshah (Kurdistan Iranien): Reconstitution paléogéographique, évolution géodynamique, magmatique et structural. PhD thesis, Université Paris-Sud.

Casciello, E., Vergés, J., Saura, E., Casini, G., Fernández, N., Blanc, E., et al. (2009). Fold patterns and multilayer rheology of the Lurestan Province, Zagros simply folded belt (Iran). *Journal of the Geological Society*, *166*(5), 947–959. https://doi.org/10.1144/0016-76492008-138

Casini, G., Casciello, E., Saura, E., Vergés, J., Fernandez, N., & Hunt, D. W. (2017). Fracture characterization in sigmoidal folds: Insights from the Siah Kuh anticline, Zagros, Iran. *AAPG Bulletin*, *102*(03), 369–399. https://doi.org/10.1306/0503171615817076

Corradetti, A., Tavani, S., Russo, M., Arbués, P. C., & Granado, P. (2017). Quantitative analysis of folds by means of orthorectified photogrammetric 3D models: A case study from Mt. Catria, Northern Apennines, Italy. *The Photogrammetric Record*, *32*(160), 480–496. https://doi.org/10.1111/phor.12212

Cowie, P. A., & Scholz, C. H. (1992). Growth of faults by accumulation of seismic slip. *Journal of Geophysical Research*, *97*(B7), 11,085–11,095. https://doi.org/10.1029/92JB00586

De Wever, P., Bourdillon-de Grissac, C., & Bechennec, F. (1988). Permian age from radiolarites of the Hawasina nappes, Oman Mountains. *Geology*, *16*(10), 912–914. https://doi.org/10.1130/0091-7613(1988)016<0912:PAFROT>2.3.CO;2

Dercourt, J., Zonenshain, L. P., Ricou, L.-E., Kazmin, V. G., Le Pichon, X., Knipper, A. L., et al. (1986). Geological evolution of the Tethys belt from the Atlantic to the Pamirs since the Lias. *Tectonophysics*, *123*(1–4), 241–315. https://doi.org/10.1016/0040-1951(86)90199-X

Franke, D. (2013). Rifting, lithosphere breakup and volcanism: Comparison of magma-poor and volcanic rifted margins. *Marine and Petroleum Geology*, *43*, 63–87. https://doi.org/10.1016/j.marpetgeo.2012.11.003

Frizon de Lamotte, D., Raulin, C., Mouchot, N., Wrobel-Daveau, J.-C., Blanpied, C., & Ringenbach, J.-C. (2011). The southernmost margin of the Tethys realm during the Mesozoic and Cenozoic: Initial geometry and timing of the inversion processes. *Tectonics*, *30*, TC3002. https://doi.org/10.1029/2010TC002691

Gardosh, M. A., Garfunkel, Z., Druckman, Y., & Buchbinder, B. (2010). Tethyan rifting in the Levant region and its role in Early Mesozoic crustal evolution. *Geological Society of London, Special Publication*, *341*(1), 9–36. https://doi.org/10.1144/SP341.2

Garfunkel, Z. (1998). Constraints on the origin and history of the Eastern Mediterranean basin. *Tectonophysics*, *298*(1–3), 5–35. https://doi.org/10.1016/S0040-1951(98)00176-0

Garfunkel, Z. (2004). Origin of the Eastern Mediterranean basin: a reevaluation. *Tectonophysics*, *391*(1–4), 11–34. https://doi.org/10.1016/j.tecto.2004.07.006

Garfunkel, Z., & Derin, B. (1984). Permian-early Mesozoic tectonism and continental margin formation in Israel and its implications for the history of the Eastern Mediterranean. *Geological Society of London, Special Publications*, *17*(1), 187–201. https://doi.org/10.1144/GSL.SP.1984.017.01.12

Gharib, F., & De Wever, P. (2010). Radiolaires mésozoïques de la formation de Kermanshah (Iran). *Comptes Rendus Palevol*, *9*(5), 209–219. https://doi.org/10.1016/j.crpv.2010.06.003

Ghasemi, A., & Talbot, C. J. (2006). A new tectonic scenario for the Sanandaj–Sirjan Zone (Iran). *Journal of Asian Earth Sciences*, *26*(6), 683–693. https://doi.org/10.1016/j.jseaes.2005.01.003

Gillard, M., Autin, J., & Manatschal, G. (2016). Fault systems at hyper-extended rifted margins and embryonic oceanic crust: Structural style, evolution and relation to magma. *Marine and Petroleum Geology*, *76*, 51–67. https://doi.org/10.1016/j.marpetgeo.2016.05.013

Hessami, K., Koyi, H. A., & Talbot, C. J. (2001). The significance of strike-slip faulting in the basement of the Zagros fold and thrust belt. *Journal of Petroleum Geology*, *241*, 5–28.

Hunziker, D., Burg, J. P., Bouilhol, P., & Quadt, A. (2015). Jurassic rifting at the Eurasian Tethys margin: Geochemical and geochronological constraints from granitoids of North Makran, southeastern Iran. *Tectonics*, *34*, 571–593. https://doi.org/10.1002/2014TC003768

Jackson, J. A. (1980). Reactivation of basement faults and crustal shortening in orogenic belts. *Nature*, *283*(5745), 343–346. https://doi.org/10.1038/283343a0

Jahani, S., Callot, J. P., Letouzey, J., & Frizon de Lamotte, D. (2009). The eastern termination of the Zagros Fold-and-Thrust Belt, Iran: Structures, evolution, and relationships between salt plugs, folding, and faulting. *Tectonics*, *28*, TC6004. https://doi.org/10.1029/2008TC002418

James, G. A., & Wynd, J. G. (1965). Stratigraphic nomenclature of Iranian Oil Consortium Agreement Area. *AAPG Bulletin*, *49*, 2182–2245.

Jassim, S. Z., & Buday, T. (2006). Late Eocene-Recent megasequences. In S. Z. Jassim & J. C. Goff (Eds.), *Geology of Iraq* (chap. 14, pp. 228–253). Prague and Moravian Museum, Brno: Publication of Dolin.

Jassim, S. Z., & Goff, J. C. (2006). *Geology of Iraq*. Brno, Czech Republic: DOLIN, distributed by Geological Society of London.

Kazmin, V. G., Ricou, L. E., & Sbortshikov, I. M. (1986). Structure and evolution of the passive margin of the eastern Tethys. *Tectonophysics*, *123*(1–4), 153–179. https://doi.org/10.1016/0040-1951(86)90196-4

Kim, Y. S., & Sanderson, D. J. (2005). The relationship between displacement and length of faults: A review. *Earth-Science Reviews*, *68*(3–4), 317–334. https://doi.org/10.1016/j.earscirev.2004.06.003

Koop, W. J., & Stoneley, R. (1982). Subsidence history of the Middle East Zagros basin, Permian to recent. *Philosophical Transactions of the Royal Society of London A: Mathematical, Physical and Engineering Sciences*, *305*(1489), 149–168. https://doi.org/10.1098/rsta.1982.0031

Koshnaw, R. I., Horton, B. K., Stockli, D. F., Barber, D. E., Tamar-Agha, M. Y., & Kendall, J. J. (2017). Neogene shortening and exhumation of the Zagros fold-thrust belt and foreland basin in the Kurdistan region of northern Iraq. *Tectonophysics*, *694*, 332–355. https://doi.org/10.1016/j.tecto.2016.11.016

Lacombe, O., Bellahsen, N., & Mouthereau, F. (2011). Fracture patterns in the Zagros Simply Folded Belt (Fars, Iran): Constraints on early collisional tectonic history and role of basement faults. *Geological Magazine*, *148*(5–6), 940–963. https://doi.org/10.1017/S001675681100029X

Mattioli, E., & Erba, E. (1999). Synthesis of calcareous nannofossil events in the Tethyan Jurassic. *Rivista Italiana di Paleontologia e Stratigrafia*, *105*(3), 343–376.

McQuarrie, N., & van Hinsbergen, D. J. J. (2013). Retrodeforming the Arabia-Eurasia collision zone: Age of collision versus magnitude of continental subduction. *Geology*, *41*(3), 315–318. https://doi.org/10.1130/G33591.1

Moghadam, H. S., & Stern, R. J. (2011). Late Cretaceous forearc ophiolites of Iran. *Island Arc*, *20*(1), 1–4. https://doi.org/10.1111/j.1440-1738.2010.00745.x

Moghadam, H. S., & Stern, R. J. (2015). Ophiolites of Iran: Keys to understanding the tectonic evolution of SW Asia: (II) Mesozoic ophiolites. *Journal of Asian Earth Sciences*, *100*, 31–59. https://doi.org/10.1016/j.jseaes.2014.12.016

Molinaro, M., Leturmy, P., Guezou, J.-C., Frizon de Lamotte, D., & Eshraghi, S. A. (2005). The structure and kinematics of the southeastern Zagros fold-thrust belt, Iran: From thin-skinned to thick-skinned tectonics. *Tectonics*, *24*, TC3007. https://doi.org/10.1029/2004TC001633

Mouthereau, F., Lacombe, O., & Vergés, J. (2012). Building the Zagros collisional orogen: Timing, strain distribution and the dynamics of Arabia/Eurasia plate convergence. *Tectonophysics*, *532*, 27–60.

Muttoni, G., Mattei, M., Balini, M., Zanchi, A., Gaetani, M., & Berra, F. (2009). The drift history of Iran from the Ordovician to the Triassic. *Geological Society, London, Special Publications*, *312*(1), 7–29. https://doi.org/10.1144/SP312.2

Navabpour, P., Angelier, J., & Barrier, E. (2011). Brittle tectonic reconstruction of palaeo-extension inherited from Mesozoic rifting in West Zagros (Kermanshah, Iran). *Journal of the Geological Society*, *168*(4), 979–994. https://doi.org/10.1144/0016-76492010-108

Ricou, L. E., Braud, J., & Brunn, J. H. (1977). Le Zagros, Mémoires de la Société Géologique de France 8, 33–52.

Robertson, A. H. F. (2007). Overview of tectonic settings related to the rifting and opening of Mesozoic ocean basins in the Eastern Tethys: Oman, Himalayas and Eastern Mediterranean regions. *Geological Society of London, Special Publication*, *282*(1), 325–388. https://doi.org/10.1144/SP282.15

Robin, C., Gorican, S., Guillocheau, F., Razin, P., Dromart, G., & Mosaffa, H. (2010). Mesozoic deep-water carbonate deposits from the southern Tethyan passive margin in Iran (Pichakun nappes, Neyriz area): Biostratigraphy, facies sedimentology and sequence stratigraphy. *Geological Society of London, Special Publication*, *330*(1), 179–210. https://doi.org/10.1144/SP330.10

Saccani, E., Allahyari, K., Beccaluva, L., & Bianchini, G. (2013). Geochemistry and petrology of the Kermanshah ophiolites (Iran): Implication for the interaction between passive rifting, oceanic accretion, and OIB-type components in the Southern Neo-Tethys Ocean. *Gondwana Research*, *24*(1), 392–411. https://doi.org/10.1016/j.gr.2012.10.009

Sadeghi, S., & Yassaghi, A. (2016). Spatial evolution of Zagros collision zone in Kurdistan, NW Iran: Constraints on Arabia–Eurasia oblique convergence. *Solid Earth*, *7*(2), 659–672. https://doi.org/10.5194/se-7-659-2016

Salvini, F., & Vittori, E. (1982). Analisi strutturale della linea Olevano-Antrodoco-Posta (Ancona-Anzio Auct.): Metodologia di studio delle deformazioni fragili e presentazione del tratto meridionale. *Memorie della Societa Geologica Italiana*, *24*, 337–355.

Saura, E., Vergés, J., Homke, S., Blanc, E., Serra-Kiel, J., Bernaola, G., et al. (2011). Basin architecture and growth folding of the NW Zagros early foreland basin during the Late Cretaceous and early Tertiary. *Journal of the Geological Society*, *168*(1), 235–250. https://doi.org/10.1144/0016-76492010-092

Sengör, A. M. C. (1979). Mid-Mesozoic closure of Permo-Triassic Tethys and its implications. *Nature*, *279*(5714), 590–593. https://doi.org/10.1038/279590a0

Sengör, A. M. C., & Yilmaz, Y. (1981). Tethyan evolution of Turkey—A plate tectonic approach. *Tectonophysics*, *75*(3–4), 181–241. https://doi.org/10.1016/0040-1951(81)90275-4

Sepehr, M., & Cosgrove, J. W. (2004). Structural framework of the Zagros fold–thrust belt, Iran. *Marine and Petroleum Geology*, *21*(7), 829–843. https://doi.org/10.1016/j.marpetgeo.2003.07.006

Sherkati, S., & Letouzey, J. (2004). Variation of structural style and basin evolution in the central Zagros (Izeh zone and Dezful Embayment), Iran. *Marine and Petroleum Geology*, *21*(5), 535–554. https://doi.org/10.1016/j.marpetgeo.2004.01.007

Sherkati, S., Molinaro, M., Frizon de Lamotte, D., & Letouzey, J. (2005). Detachment folding in the Central and Eastern Zagros fold-belt (Iran): Salt mobility, multiple detachments and late basement control. *Journal of Structural Geology*, *27*(9), 1680–1696. https://doi.org/10.1016/j.jsg.2005.05.010

Snidero, M., Amilibia, A., Gratacos, O., Blanc, E. P., & Muñoz, J. A. (2011). The 3D reconstruction of geological structures based on remote sensing data: Example from the Anaran anticline, Lurestan province, Zagros fold and thrust belt, Iran. *Journal of the Geological Society*, *168*(3), 769–782. https://doi.org/10.1144/0016-76492010-107

Stampfli, G. M., & Borel, G. D. (2002). A plate tectonic model for the Paleozoic and Mesozoic constrained by dynamic plate boundaries and restored synthetic oceanic isochrons. *Earth and Planetary Science Letters*, *196*(1–2), 17–33. https://doi.org/10.1016/S0012-821X(01)00588-X

Stöcklin, J. (1968). Structural history and tectonics of Iran: A review. *AAPG Bulletin*, *52*, 1229–1258.

Szabo, F., & Kheradpir, A. (1978). Permian and Triassic stratigraphy, Zagros basin, South-West Iran. *Journal of Petroleum Geology*, *1*(2), 57–82. https://doi.org/10.1111/j.1747-5457.1978.tb00611.x

Talbot, C. J., & Alavi, M. (1996). The past of a future syntaxis across the Zagros. *Geological Society of London, Special Publication*, *100*(1), 89–109. https://doi.org/10.1144/GSL.SP.1996.100.01.08

Tavakoli-Shirazi, S., Frizon de Lamotte, F., Wrobel-Daveau, J. C., & Ringenbach, J. C. (2013). Pre-Permian uplift and diffuse extensional deformation in the High Zagros Belt (Iran): Integration in the geodynamic evolution of the Arabian plate. *Arabian Journal of Geosciences*, *6*(7), 2329–2342. https://doi.org/10.1007/s12517-012-0542-5

Tavani, S., Corradetti, A., & Billi, A. (2016). High precision analysis of an embryonic extensional fault-related fold using 3D orthorectified virtual outcrops: The viewpoint importance in structural geology. *Journal of Structural Geology*, *86*, 200–210. https://doi.org/10.1016/j.jsg.2016.03.009

Tavani, S., Granado, P., Corradetti, A., Girundo, M., Iannace, A., Arbués, P., et al. (2014). Building a virtual outcrop, extracting geological information from it, and sharing the results in Google Earth via OpenPlot and Photoscan: An example from the Khaviz Anticline (Iran). *Computers & Geosciences*, *63*, 44–53. https://doi.org/10.1016/j.cageo.2013.10.013

Tavani, S., Mencos, J., Bausà, J., & Muñoz, J. A. (2011). The fracture pattern of the Sant Corneli Bóixols oblique inversion anticline (Spanish Pyrenees). *Journal of Structural Geology*, *33*(11), 1662–1680. https://doi.org/10.1016/j.jsg.2011.08.007

Tavani, S., Parente, M., Puzone, F., Corradetti, A., Gharabeigli, G., Valinejad, M., et al. (2018). The seismogenic fault system of the 2017 Mw 7.3 Iran-Iraq earthquake: Constraints from surface and subsurface data, cross-section balancing and restoration. *Solid Earth*, *9*, 821–831.

van Bellen, R.C., Dunnington, H.V., Wetzel, R., Morton, D.M., Dubertret, L., 1959. Stratigraphic lexicon of Iraq. Lexique stratigraphique International III, Asie, fasc 10a, Iraq. CNRS Paris.

van Buchem, F. S., Al-Husseini, M. I., Maurer, F., Droste, H. J., & Yose, L. A. (2010). Sequence-stratigraphic synthesis of the Barremian–Aptian of the eastern Arabian Plate and implications for the petroleum habitat. Barremian-Aptian stratigraphy and hydrocarbon habitat of the eastern Arabian Plate. *GeoArabia Special Publication*, *4*, 9–48.

Vergés, J., Saura, E., Casciello, E., Fernàndez, M., Villaseñor, A., Jiménez-Munt, I., & García-Castellanos, D. (2011). Crustal-scale cross-sections across the NW Zagros belt: Implications for the Arabian margin reconstruction. *Geological Magazine*, *148*(5–6), 739–761. https://doi.org/10.1017/S0016756811000331

Verhoeven, G. (2011). Taking computer vision aloft-archaeological three-dimensional reconstructions from aerial photographs with Photoscan. *Archaeological Prospection*, *18*(1), 67–73. https://doi.org/10.1002/arp.399

Wrobel-Daveau, J.-C., Ringenbach, J.-C., Tavakoli, S., Ruiz, G. M. H., Masse, P., & Frizon de Lamotte, D. (2010). Evidence for mantle exhumation along the Arabian margin in the Zagros (Kermanshah area, Iran). *Arabian Journal of Geosciences*, *3*(4), 499–513. https://doi.org/10.1007/s12517-010-0209-z

Ziegler, M. A. (2001). Late Permian to Holocene paleofacies evolution of the Arabian Plate and its hydrocarbon occurrences. *GeoArabia*, *6*, 445–504.

Ziegler, P. A., & Cloetingh, S. (2004). Dynamic processes controlling evolution of rifted basins. *Earth-Science Reviews*, *64*(1–2), 1–50. https://doi.org/10.1016/S0012-8252(03)00041-2